Low Temperature Study of The Exciton Diffusion in Conjugated Polymers

Master thesis by

Oleksandr Mikhnenko

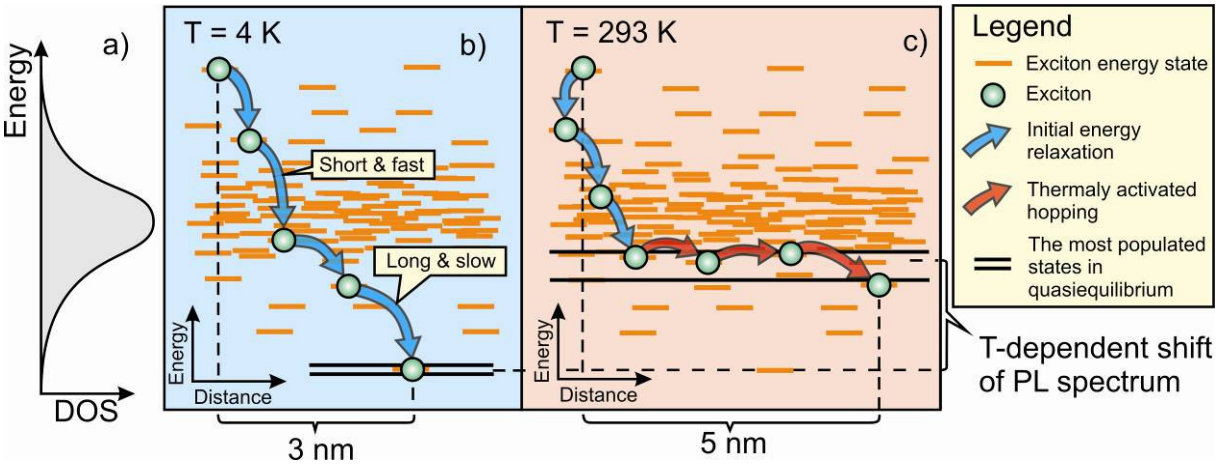

Group Leader: Prof. Dr. Paul W. M. Blom
Supervisor: Dr. Maria-Antonietta Loi
Referent: Dr. Beatriz Noheda
Period: September 2006 – August 2007
Credits: 54 ECTC

University of Groningen
Zernike Institute for Advanced Materials

Groningen, 2007

ABSTRACT

Excitonic processes in soluble derivatives of polyphenylene-vinylene (PPV) were studied by the means of time-resolved spectroscopy in the temperature range of 4-293K. The photoluminescence decay times of reference pristine PPV thin films were compared with the ones of the film with an exciton quenching interface. Such an interface is formed by spin-casting PPV derivative on top of insoluble fullerene-based polymerized exciton quenching layer. It was demonstrated that the free interface of spin-coat MEH- and MDMO-PPV films also quenches exitons with efficiency comparable to the polymer-fullerene interface. The experimental data were fit with 1D diffusion model to extract both the exciton diffusion length and the diffusion coefficient. The temperature dependence of the exciton diffusion length (coefficient) for MDMO-PPV demonstrates two temperature regimes with different trends. Upon cooling from the room temperature to 100 K the exciton diffusion length (coefficient) drops from 4,7 nm ($3.6 \cdot 10^{-4}$ cm^2/s) to 2,9 nm ($1.5 \cdot 10^{-4}$ cm^2/s). Further cooling down to 4 K leads to a weak temperature dependence and a slight growth up to 3,2 nm ($2 \cdot 10^{-4}$ cm^2/s). The obtained results are qualitatively explained by the quasiequilibrium exciton distribution in an inhomogeneously broadened density of excited states.

INDEX

CHAPTER 1

Introduction

We can think about three types of media in our planet: water, air and soil. It appears that life forms are the most concentrated on the surface and close to the water. Its abundance is decreased rapidly when distancing from these interfaces. One could use such example to draw an analogy with a general trend that occurs in the science during the last decades. A lot of interesting results were obtained at the border of the conventional natural sciences namely physics, chemistry and biology. Such an interdisciplinary approach gives rise to new scientific fields such as nanoscience, mesoscopic physics, biochemistry, molecular electronics etc. The advances in these new fields opened the door to conceptually new applications and devices like nanorobots, addressed drug delivery, quantum cryptography, flexible displays, inkjet printed electronics etc.

The field of organic semiconductors is developed on the border of chemistry and physics. The possibility of chemical tuning of the fundamental physical properties is one of the most important advantages of the organic semiconductors compared to conventional inorganic materials. Another promising property of organics is flexibility. Flexible devices could be made with active layer and substrate both organic. For instance, a purely organic active matrix display was recently reported [1]. Organic materials are much

lighter than inorganic semiconductors. This property is very important in some cases. For example, the solar powered aircraft (Fig. 1.1) requires lightweight solar cells to fly efficiently. Such solar cells could be created by use of organic materials on plastic substrates.

Fig. 1.1. Prototype of the solar powered aircraft [3].

Easy processing and the low cost of organic materials make various commercial applications promising. A number of different devices like organic light emitting diode (LED), photovoltaic cell, field effect transistor (FET), organic memory etc. were designed using organic semiconductors. Some of them are now approaching the market as products. Electrical circuits could be simply inkjet printed using organic semiconductor ink [2]. This technology gives rise to fantastic applications. Animated newspapers like in the Harry Potter movies could be in principal fabricated.

Despite all named advantages devices based on the organic semiconductors do not demonstrate high performances due to low purity and low charge carrier mobility. Therefore in the most cases they could be commercially used only if the low price and high quantity are more important than performances.

In the present work we concentrated on two soluble PPV-derivatives (poly(p-phenylene-vinylene)). These polymers are used as active layer of organic FETs, LEDs and solar cells. Our aim was to study the important fundamental physical process of the exciton diffusion at various temperatures. The exciton diffusion length determines the optimal morphology of the solar cells. It plays an important role in the operation of organic LEDs determining the amount of quenched excitons by the cathode. And finally it is of high fundamental interest.

CHAPTER 2

Background

In this chapter basic knowledge about the π-conjugated system is presented. In real polymers the conjugation is broken into segments due to various defects. The statistical energy distribution of the frontier molecular orbitals of such segments is responsible for inhomogeneously broadened density of states, which governs excitonic and charge conduction properties of conjugated polymers. Optical excitations in the most cases behave like Frenkel excitons, which can diffuse among conjugated segments. The exciton diffusion length is of high fundamental interest and is a very important parameter for the design of optoelectronic devices. To study the exciton diffusion process usually quenchers are implemented at a well-defined position of the sample. The photoluminescence intensity is recorded and fitting with an appropriate mathematical model allows extracting the parameters of interest.

2.1 Pi-conjugated systems

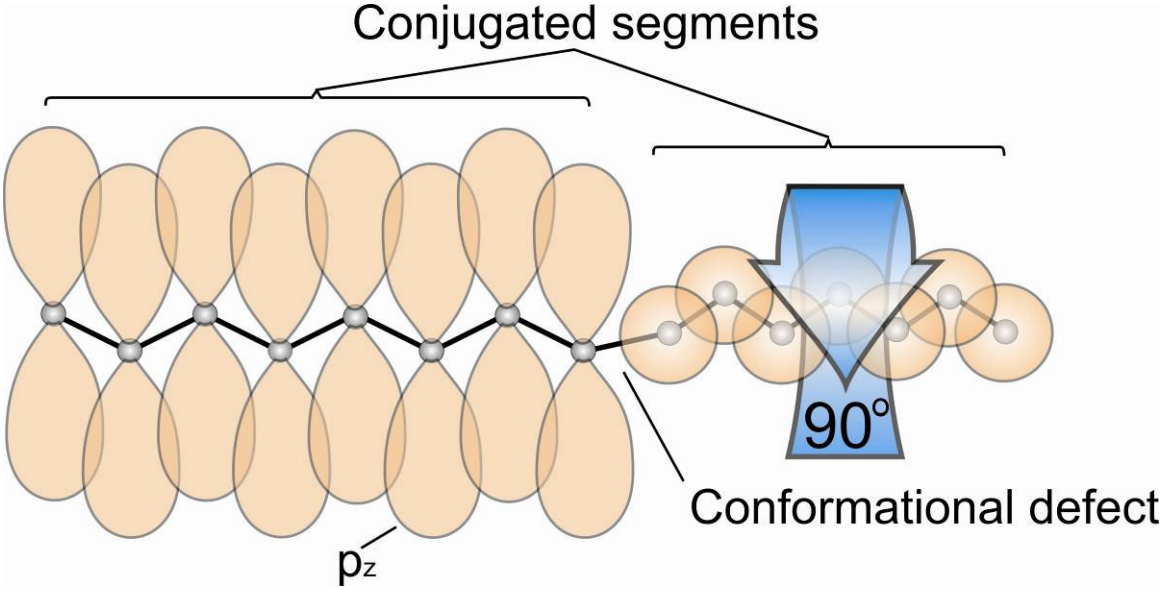

Fig. 2.2. Conjugated polymer. The double bonds are formed by the overlap of the sp^2 hybridized orbitals (black lines) and non-hybridized p_z orbitals (orange dumbbells), which point out of the molecular plane. The conjugation can be broken into segments due to various defects.

π-conjugated system is a system of atoms covalently bounded with alternating single and double bonds (–C=C–C=C–C=) in a molecule of an organic compound. Carbon atoms are sp^2 hybridized in such systems. The two bonds of the double bond are not equal. One bond is formed by the overlap of the hybridized orbitals of the adjacent atoms. Such a bond geometrically located in the molecular plane, in between of the bonding carbon atoms. Another bond is formed out of the molecular plane by the overlapping non-hybridized (p_z) atomic orbitals (Fig. 2.2). Such orbitals form an electron cloud above the molecular plane, which is responsible for spatially extended frontier molecular orbitals HOMO and LUMO[1]. These orbitals are often denoted as π and π* respectively, which explains the name "π-conjugated systems". The high interest to such compounds was risen by Shirakawa, MacDiarmid, and Heeger in 1977. They discovered high electrical conduction of oxidized polyacetylene [4] and later where awarded with the Nobel Prize in chemistry.

[1] HOMO stands for the highest occupied molecular orbital; LUMO – the lowest unoccupied molecular orbital.

The energy gap between HOMO and LUMO is a crucial parameter for the photo physical properties of organic materials. It determines the absorption and emission spectra of a molecule. In π-conjugated systems HOMO-LUMO gap depends on the length of the conjugated segment. This can be illustrated by the simple quantum mechanical problem of particle in the box. The smaller box is the bigger energy separation particle has. The conjugated segment plays a role of the box and the delocalized π-electrons are particles. Upon increase of the conjugation length the HOMO-LUMO gap gets smaller (Fig. 2.3). The infinite conjugated chain would have the smallest energy separation. The frontier orbitals would transform to the bands and the chain would become one-dimensional semiconductor. Therefore π-conjugated systems are often called organic semiconductors and HOMO-LUMO gap sometimes is denoted as a band gap.

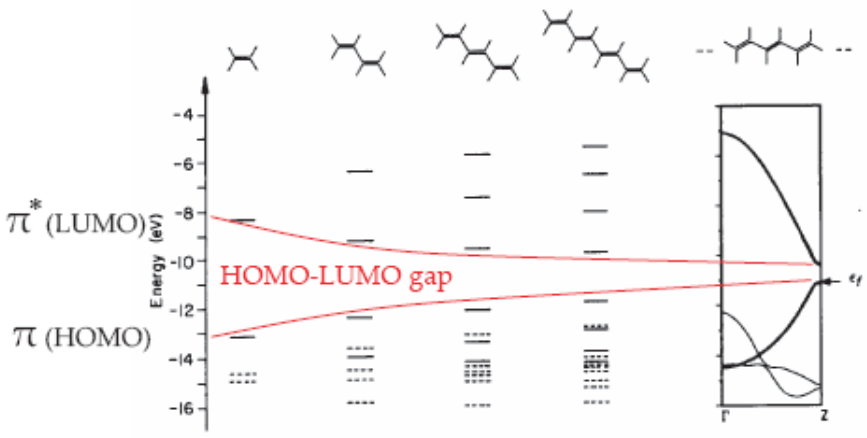

Fig. 2.3. Dependence of the HOMO-LUMO gap on the conjugated length. Bands are formed in the infinite conjugated chain.

The charge conduction along the infinite conjugated chain follows the same mechanism as in the intrinsic inorganic semiconductors. Electrons from the valence band (former HOMO) could be promoted to the conduction band (former LUMO) and easily transported along the chain. This process is called band conduction. In real polymers the conjugation of a long chain is broken into segments due to various defects (Fig. 2.2). Assemble of such segments can not be described in terms of bands. Statistical distribution of HOMOs and LUMOs determines inhomogeneously broadened density of states, which is

proper energetical description of a real polymer [5]. Charge conduction is realized by hoping from one conjugated segment to another.

Despite in theory organic materials are expected to conduct both electrons and holes, in practice they usually behave as either electron or hole conductors. Very few organic materials are known to have intrinsic ambipolar transport [6, 7].

2.2 The exciton diffusion process

Due to the disorder and low dielectric constant an optical excitation in the conjugated polymers can be described as the localized Frenkel-like excitation [5]. The area of localization of the photo excitation is usually limited by a single conjugated segment [8, 9]. Interchain excitations are also possible involving several adjacent segments [10-12]. After its formation the exciton is involved in a complicated process that is called exciton life. We concentrate our effort to study the important properties of this process.

Despite its lifetime is relatively short – of the order of 1 ns in PPV derivatives – the process of the exciton evolution plays a crucial role, for instance, in the solar cells. Since electron and hole are strongly bounded (of the order of 10kT at room temperature [17]) charge separation is required for the photovoltaic effect. It is commonly done by the use of two materials with appropriate HOMO-LUMO gap (Fig. 2.4). One of the two materials conducts holes (AKA positive polarons or radical cation) and another has electron (AKA negative polaron or radical anion) conducting properties. Conjugated polymers and fullerenes are known to satisfy such requirements [13]. The charge transfer occurs with high probability at the interface of these materials. Separated charges can be extracted then by electrodes attached to the active layer with appropriate work functions. Thus current can be obtained from the excitons that during their lifetime reach the interface between the two materials. Therefore the average distance of exciton migration is one of the parameters determining the efficiency of the solar cells. In order to increase

the area of the interface special morphology of the active layer is used called bulk heterojunction [14]. Instead of well defined layers of the electron and hole conducting materials interpenetrated network is designed. In this case exciton diffusion length determines the optimal morphology of the bulk heterojunction.

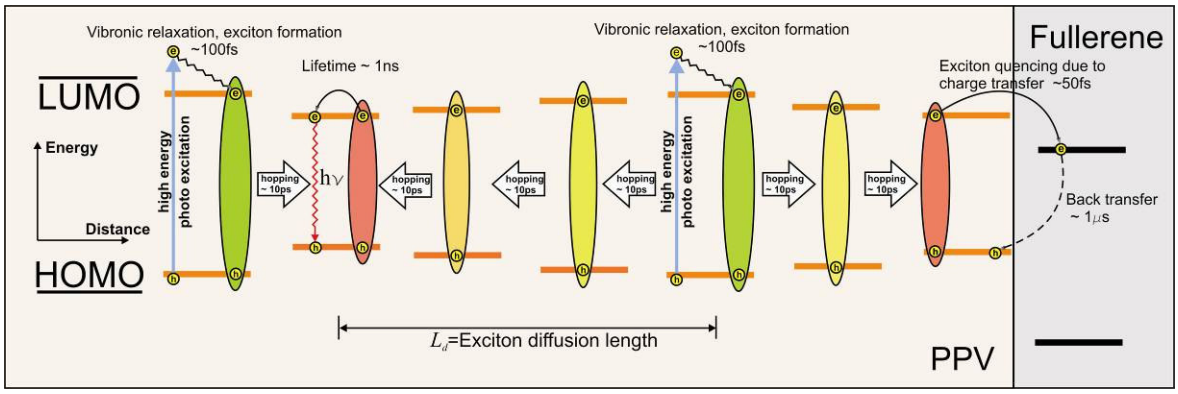

Fig. 2.4. Evolution of the excitons in polymer. Polymer segments with different conjugation length are depicted as separate chromophores with different energy levels. The process of the exciton quenching at polymer-fullerene interface is illustrated. Note, that the photon absorption is oversimplified on this cartoon. In reality electron is lifted to LUMO from the HOMO level (black lines). Electron-hole pair then relaxes to form an exciton (orange lines).

The evolution of the optical excitations is schematically depicted at the Figure 2.4. The photon absorption is followed by the rapid vibronic relaxation and the exciton formation. In this case we assume that the excitation is performed at high energy tail of the absorption spectrum. Thus the shortest conjugated segments are excited. They are surrounded with the segments of the longer conjugation. It is energetically favorable to transfer excitation to such a segment. Such process is believed to have mainly Förster-type energy transfer nature (see [15] and references inside) and it is responsible for the large Stokes shift of the photoluminescence spectrum in polymers. Thus excitons rapidly migrate towards sites with lower energy with the hopping rate of the order of 10ps [16-18] or even faster [19]. Finally they reach the lowest energy site in the neighborhood where radiative or non-radiative decay happens. Another possibility is exciton quenching due to the charge transfer. For instance, electron transfer can occur at fullerene-polymer interface within 50 fs, while the back transfer is of the order of milliseconds [20, 21, 28]. This

process is employed in solar cells and used in our work to study the exciton diffusion process.

The model described here is oversimplified. It does not include processes like interchain excitation [10-12], exciton-exciton annihilation [35], intersystem crossing etc. However, the real physical picture of the exciton life in conjugated polymers is still under debate. Some attempts to describe it can be found in [12] and [22]. The most important thing for this introduction is that excitons undergo migration in conjugated polymers.

Since the polymer media is highly disordered the exciton migration can be sufficiently described by random walk approximation [8, 9, 37]. As it would be demonstrated below at room temperature it is possible to approximate it as a diffusion process. Nowadays the term *exciton diffusion* is commonly used in the literature to denote exciton migration in conjugated polymers.

Our main interest is to study the exciton diffusion length in conjugated polymers. The exciton diffusion length can be defined as the average distance an exciton can travel before it decays. It depends on the exciton lifetime τ, exciton diffusion coefficient D and dimensionality of the diffusion process d:

$$L_d = \sqrt{d\tau D}\,. \tag{2.1}$$

d is equal to unity for the one dimensional diffusion.

2.3 Experimental techniques: advantages and disadvantages

The generally used technique to probe the exciton diffusion length suggests sample fabrication with exciton quenchers implemented in the material of interest at a well-defined spatial position. Due to the presence of the quenchers photoluminescence of the sample is weaker and PL decay time is shorter then that of pristine material. Time-resolved or steady state PL data can be used to calculate the relative quenching efficiency:

$$Q = 1 - \frac{Total\ PL\ of\ the\ quenched\ sample}{Total\ PL\ of\ the\ reference\ sample}. \qquad (2.2)$$

Here the total photoluminescence represents the total number of photons emitted (per excitation pulse or per unit of time). The relative quenching efficiency can be used in the mathematical model that includes the sample geometry in order to extract the exciton diffusion length, which is usually the only fit parameter in such models.

Two suitable geometries for such experiments are homogeneous quencher distribution in bulk and the interface quenching of the thin film heterostructures.

Thus by varying the optical technique and the sample geometry it is possible to perform several different experiments to study the exciton diffusion process. Each of these methods shows both advantages and disadvantages.

In steady state experiments sample is excited by a constant wave laser. The absolute photoluminescence intensity is measured usually by integrating sphere or a spectrometer [24-27]. Unfortunately it is quite difficult to conduct this experiment. It is very sensitive to the alignment of the optical system and high power stability is required. Also the self-absorption can influence the resulting PL intensity for thicker samples. The integrating sphere usually can not operate at low temperatures. In steady state experiment it is possible to measure the exciton diffusion length. However it is not possible to extract the exciton diffusion coefficient out of the experimental data.

The exciton diffusion coefficient can be extracted from the **photoluminescence decay** [22, 28-30]. In this experiment the sample is excited by a pulsed laser. The total photoluminescence (2.2) is the time integral of the photoluminescence decay. It is weakly dependent on the experimental conditions because the maximum value of the PL decay can be normalized. Thus this approach does not have the absolute intensity problem appearing in the steady state experiments. However due to finite instrument

response function (rise time) uncertainty of the maximum value of PL intensity at the moment just after the excitation ($t = 0$) appears. Consequently the assumption of equal normalized PL intensity at $t = 0$ can be a source of errors for the integrated value.

Another problem of normalization arises when it is measured the PL decay of highly quenched samples. One expects all mobile excitons to be quenched in this case. However some localized conjugated fragments can be present. They have the nearest neighbors with much higher HOMO-LUMO gap. This makes an exciton to be trapped at such a segment. Its lifetime is expected to be of the order of the natural PL decay. The contribution to the total (very weak) PL of such conjugated segments can become valuable. The normalization to unity can enhance this artifact making the time integral bigger than the physically correct value.

A soluble fullerene derivative is commonly used in practice to create **homogeneous exciton quencher distribution** in the bulk of a conjugated polymer sample [36]. Fullerenes are blended to the solution of the material under study. Then a thin film is created by the spin-coating technique. Photoluminescence measurements are performed on the blend and on the reference sample (pristine material). Knowing the initial concentrations of the components the average distances between the quenchers could be estimated. This data are required by the mathematical model [37, 38] that yields to the exciton diffusion parameters. The problem of such approach originates from the assumption of homogenous distribution of the quenchers in the bulk material. Since the quencher's concentration is very low it is very hard to verify the homogeneous distribution. In fact the quenchers can form clusters that will effectively increase the distances between quenching centers. Due to the complicity of the mathematical model only the tail of time-resolved data can be used to extract parameters of exciton diffusion [36]. The valuable advantage of this geometry is that the sample is isotropic, allowing to probe the tree-dimensional diffusion process.

Another important approach is to use **interface quenching** to study exciton diffusion. In this case thin films have one or both interfaces connected to an exciton quenching material. Generally for such a purpose fullerenes [22, 28-30], metals [26] or oxides [27] are selected for the role of quenchers. With this geometry the PL of the thinner films decays faster and has lower total intensity compared to the appropriate reference sample. This geometry requires a sharp interface between the material of interest and the quencher. Such requirement limits the use of evaporation technique for the quencher deposition. For instance, it is shown that evaporated fullerenes can diffuse into the polymer film [30]. As it will be elucidated in the following chapters, some thickness and free interface effects can introduce extra artifacts. This geometry is well defined and all the distances are under control. Due to anisotropic orientation of the long polymer chains [31] such sample configuration allows probing exciton diffusion only in one dimension, perpendicular to the film. However, it was shown [36] that exciton migration occurs primary with interchain mechanism, normal to the thin film.

Besides "quenching techniques" some other methods have been developed to study singlet exciton diffusion. They include photocurrent spectra (see [32] and references within) and exciton-exciton annihilation [35].

The photocurrent spectrum is the variation of the short circuit current of photovoltaic cell by function of the incident monochromatic photon energy. As it was mentioned above, the excitons are primary optical excitations in organic materials. The photovoltaic effect happens due to exciton dissociation near the interface between the light absorbing material and a suitable electron accepting material like fullerene, metal etc. Let's suppose one fabricates a simple photovoltaic cell with two electrodes and a thin polymer film in between. It is not likely that such device will break the efficiency record in the field, but it can be used for the exciton diffusion length measurement. Upon optical excitation excitons are created (mostly) homogeneously in the film. Those that are in the vicinity of the electrodes will rapidly dissociate contributing the photocurrent. Excitons from the bulk will

then diffuse upon interfaces to repeat the fate of their dissociated colleagues. Thus the actual value of the photocurrent depends on the exciton diffusion length. Naturally it also depends on the absorption coefficient of the material at the excitation wavelength. By modeling the photocurrent spectrum it is possible to extract the exciton diffusion coefficient [32-34, 39]. The advantage of this method is that in principal it allows probing exciton diffusion properties on a working device. The drawbacks are complexity of the sample structure/preparation and sophisticated mathematical model that should be applied. The existence of the metal electrodes implies high reflectivity of the interfaces. This leads to significant optical interference effect and extra complications. Also the quenching efficiency of the electrodes can be questionable.

Exciton-exciton annihilation appears to be diffusion-limited in conjugated polymers [35]. Or, by other words, this process takes place not directly after excitation, but during the exciton diffusion process. Recording time-dependent photoluminescence one can extract singlet-singlet annihilation constant that is proportional to the exciton diffusion coefficient. The exciton annihilation radius is proportionality constant in this dependence. Generally speaking it is not known. Lewis *et al.* made a reasonable estimation [35]. The exciton diffusion length is then determined by use of the relationship (2.1), where τ was equal to the time constant of one-exponential approximation of the PL decay at low excitation power. The advantage of this method is that the exciton diffusion coefficient corresponds to three-dimensional process, unlike in interface quenching experiment. However, high power excitation is required that can cause degradation of the sample. The main disadvantage of this method is that the exciton diffusion parameters are extracted not directly but through the estimation of the annihilation radius.

CHAPTER 3

Experimental

We applied time-resolved spectroscopy to the samples with interface quenching geometry to study the exciton diffusion process. The interface quenching was realized by preparing heterostructures of the studied materials and the insoluble cross-linked fullerene layer. The corresponding thicknesses were measured by atomic force microcopy and reflection nulling-zone ellipsometry. Sample preparation and optical measurements were performed either under inert nitrogen atmosphere or under vacuum in a cryostat to avoid photo oxidation. The temperature dependent measurements were done in the temperature range of 4-293K in a cryostat under constant helium flow.

3.1 Selection of the experimental methods

As explained in the previous section, there is no the perfect method to study the exciton diffusion process in conjugated polymers. Or at least such a method is not known jet. All suggested techniques have their advantages and disadvantages. In our experiment we choose to keep the mathematical model and the sample preparation reasonably simple and to reduce the number of estimated parameters and assumptions.

From this point of view the photocurrent method appears to be too complicated. It involves device fabrication and sophisticated mathematical modeling. The technique based on the exciton-exciton annihilation process is not very attractive because of the possible sample degradation. It also requires estimation of the exciton-exciton annihilation radius in order to extract the exciton diffusion parameters. So we considered only methods involving samples with exciton quenchers.

The use of samples with a homogeneous quencher distribution implies the assumption that quenchers do not form clusters. Also the mathematical model, in this case, is quite complicated. Due to the model assumption only the tail of PL decay can be used to extract the exciton diffusion parameters. Since conjugated polymers are known to have non-exponential decay in solid state [22] this argument leads to neglecting some of the fast physical processes.

The interface quenching appears to be the most attractive geometry for our experiments as long as sharp interfaces could be created. Time-resolved technique has been chosen to measure photoluminescence.

3.2 Samples preparation

The exciton diffusion process in two soluble derivatives of poly(p-phenylene-vinylene) (PPV) has been studied. Their chemical structures are

summarized in Figure 3.1. In text we will refer to them as MEH-PPV and MDMO-PPV.

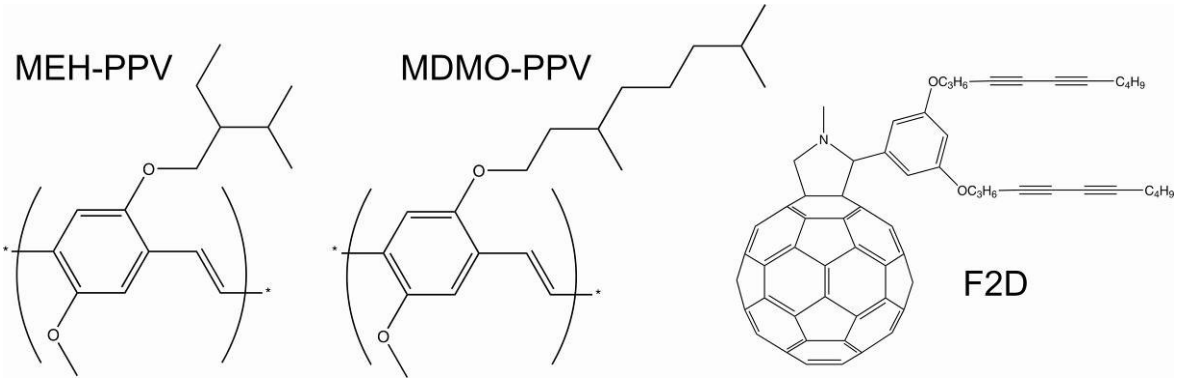

Fig. 3.1 **MEH-PPV**, poly[2-methoxy-5-(3,7-dimethyloctyloxy)]-1,4-phenylenevinylene); **MDMO-PPV**, poly[2-methyl-5-(3',7'-. dimethyloctyloxy)-p-phenylenevinylene]; **F2D**, 1'-methyl-1',5'-dihydro-2'-(3,5-bis(undeca-4,6-diynyloxy)phenyl-*1H*-pyrrolo[3',4':1,9](C_{60}-I_h)[5,6]fullerene

Two types of samples were fabricated with both materials. The thin films of the pristine materials constitute the first type of samples used in this work. They were fabricated with spin-coating technique under nitrogen atmosphere. Toluene and chlorobenzene were used as solvents for MEH- and MDMO-PPV respectively. Thickness variation was ensured by changing the solution concentration, keeping the same the spin program. All samples were spun on clean quartz substrates. The cleaning procedure includes hand scrubbing with soap; washing with the demineralized water; ultrasonic acetone and propanol baths; UV-ozone reactor treatment. The surfaces of the clean substrates and the spin-coat films were imaged by the atomic force microscopy (AFM). Roughness calculated as the standard deviation from the average level on the area of 100 μm^2 was less than 1 nm for all the surfaces.

The second type of samples is composed of bi-layer heterostructures (Fig. 3.2). First the diacetylene fullerene derivative[1] F2D (Fig. 3.1) was spun from chlorobenzene to the clean quartz substrate. Such a material is known to polymerize at 175°C forming an insoluble cross-linked network [30]. Thin films were annealed at 250°C for 20 min on the hotplate inside a nitrogen

[1] The synthesis and basic characterization of the diacetylene fullerene derivative F2D can be founded elsewhere [30]

glove box. The resulting thickness of the poly-(F2D) layer was kept the same, less than 30 nm in all the experiments. With this thickness we do not expect any optical interference effects in the visible region. Then the samples were completed by spun on top of poly-(F2D) layer a PPV derivative. The roughnesses of all the surfaces including the poly-(F2D) layer were less than 1 nm.

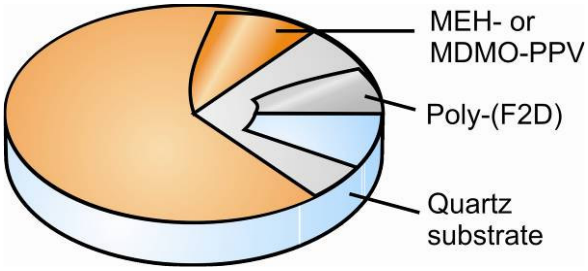

Fig. 3.2 Heterostructure. Thickness of the poly-(F2D) is less then 30 nm in all experiments. Polymer is of variable thickness.

The interface between poly-(F2D) and PPV derivative plays the role of exciton quenching wall. Since poly-(F2D) is not soluble even in the "aggressive" organic solvents like chlorobenzene and chlorophorm, the quenching interface remains sharp in time. This does not hold, for instance, in case of evaporated fullerenes on top of spin-coat polymer film. It was demonstrated [30] that fullerenes tend to diffuse towards the bulk of the film resulting ill-defined structures.

We also tried to deposit C_{70} instead of C_{60} on top of the thin film of MDMO-PPV. Despite the molecules of C_{70} are bigger, they still diffused into the polymer.

3.3 Thickness measurements

As it was mentioned in the previous chapter, one of the advantages of the interface quenching approach is the well defined geometry. The only geometrical parameter that is required by mathematical model – the polymer thickness – can be measured directly. This makes thickness measurements of crucial importance.

Polymer films as thin as 5 nm were used for our experiments. To measure thicknesses of such thin films we used two methods that can reach

required precision: atomic force microscopy (AFM) and nulling zone ellipsometry.

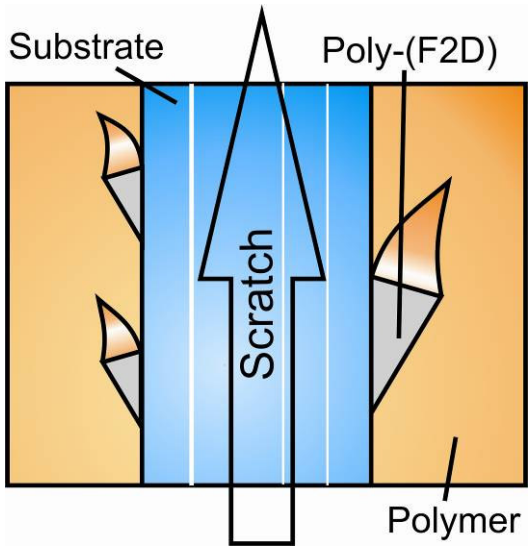

Fig. 3.3 A lucky-lucky scratch. Top view.

The thickness measuring procedure by AFM is quite straightforward for the pristine polymer films. First it is necessary to scratch the sample. A full image 10x10μm is recorded from the step area, then the step profile is averaged, leveled and the thickness is evaluated. The lucky scratch should have some step area free form the spike, which is often formed by the residuals of material that is being removed on scratching. It is quite easy to make such a scratch with polymer films. This is because the polymer tends to fold aside rather than to be removed by the scalpel.

Actually the procedure remains straightforward even with heterostructures. The only difference is that in this case one should make a lucky-lucky scratch. The heterostructure consists of the two materials with different mechanical properties. As for pristine samples, the top polymer film tends to fold aside on scratching. But poly-(F2D) follows the scalpel profile (Fig. 3.3). As a result it is possible to measure the thicknesses of both layers. The validity of this method is easily revealed by checking the thickness of the poly-(F2D) film. We kept it the same for all the experiments.

Ellipsometry was also used for thickness measurements. A brief introduction to this technique is found in Ref. [40]. In our work we used a single wavelength nulling type EP^3 Nanofilm ellipsometer, which can do multiple angle of incidence (MAI) experiments. It allows us to measure both thickness and refractive index of the thin films from a single experiment. Both thicknesses of the heterostructure can be extracted by using known refractive indices. However it is not easy to conduct measurements on the transparent

thin substrates. The problem is that reflection from the bottom substrate interface can also reach the detector and interfere with the beam reflected by the thin film(s). Thick substrates do not suffer from this problem. In our experiments we effectively increased the thickness of the substrates by attaching it to a thick (1.5cm) quartz bar. Mixture of the glycerin with water has been prepared in order to match the refractive index of quartz [41]. Thus stack of the substrate with the quartz bar was optically homogeneous and no reflections from the interface were present.

The thicknesses measured with ellipsometer nicely agree with ones obtained by AFM measurements. Because of the device availability, most of the samples were measured with AFM only.

Dektak profilometry has been also used for thickness estimations of the thick reference samples.

3.4 Spectra measurements

Absorption spectra were measured for all the samples with a Perkin–Elmer 9000 spectrometer. During the experiments the sample was mounted in the environmental chamber under inert nitrogen atmosphere. Photoluminescence spectra were recorded with the sample inside a cryostat under vacuum. An Ocean Optics USB 2000 spectrometer and Hamamatsu EM-CCD digital camera were used for that purpose. Also time-resolved spectra were recorded by working in synchroscan Hamamatsu Streak camera. The spectral responsivities of the optical setups were measured with a calibrated lamp.

3.5 Time-resolved techniques

The experimental setup is schematically depicted at Fig. 3.4. The sample was excited by 100fs pulsed frequency doubled Kerr mode locked Ti-sapphire laser. The repetition rate was about 80 MHz. The laser intensity was

controlled by neutral density filter. The estimated initial exciton density in the polymer film was about 10^{13}-$10^{14}\,cm^{-3}$, that is much lower than required for the process of exciton-exciton annihilation [35]. The excitation area was about 100μm large. During the experiments the sample was mounted in the cryostat and kept in vacuum (about 10^{-6}-10^{-5} mbar). The excitation was performed normal to the free surface of the sample. Photoluminescence was gathered from the substrate side.

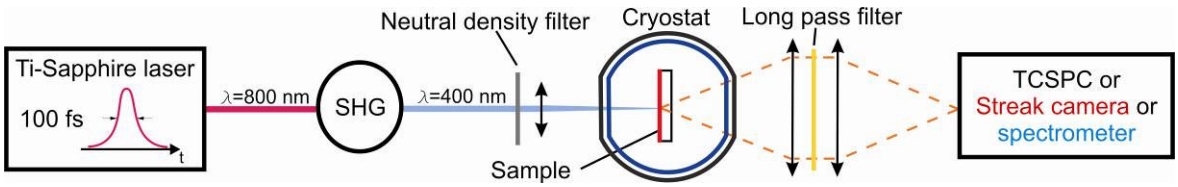

Fig. 3.4. The experimental setup for optical measurements. SHG stands for second harmonic generator, and TCSPC is time-correlated single photon counter.

Photoluminescence decays of the MEH-PPV samples were recorded with a time correlated single photon counter (TCSPC) setup. This device has response function of about 30ps (FWHM). In order to use the time-resolved data in the mathematical modeling, the PL decays were deconvoluted with the instrument response function. The measurements were performed on the wavelength that corresponds to the maximum of the PL spectra.

The samples of MDMO-PPV were measured after the lab upgrade with synchroscan Hamamatsu Streak camera. The advantage of this device is that PL decay can be recorded with the spectral resolution. In contrast to the TCSPC technique, the spectral integral of the PL decay was used in the mathematical modeling. In such a way the photons of all the energies were taken into account. Time resolution down to 2ps is achievable with such an experimental setup.

The low temperature measurements where performed with constant flow liquid helium. The heater inside of the cryostat was electronically controlled to fix a necessary temperature in the range of 4-293K.

3.6 Preventing degradation

In order to avoid the degradation processes related to water and oxygen, organic samples have been fabricated and stored under nitrogen atmosphere in the glove box. For the absorption measurements samples were sealed in an environmental chamber inside the glove box. For the time-resolved measurements samples were loaded to the cryostat and were kept under vacuum. The only moment when they were exposed to air was during the loading to the cryostat. Nevertheless during this process samples were not faced with ultraviolet light.

The excitation energy was kept low during the time-resolved experiments. Time integrated laser power did not exceed 100 μW for Streak camera measurements and 300 μW for TCSPC measurements. In order to check the possible sample degradation, it was exposed for one hour with the power of 300 μW. No change in spectrum and PL decay was detected. Half an hour laser exposition with one order of magnitude increased power led to the spectral blue shift and change of the PL decay, indicating photo degradation.

The time-resolved experiments were quite fast. Less than 1 minute was necessary for every measurement. So we are very sure that during our experiments sample did not degrade.

CHAPTER 4

Morphology effects

Two differently ordered layers of a spin-coat film were demonstrated by the absorption spectroscopy. The top layer has better ordering and is responsible for the red shift of the absorption spectrum upon thickness decrease from about 100 to 15 nm. Some other studies are listed which reveal bi-layered structure of the spin-coat films. It is demonstrated that the free interface of such prepared MEH- and MDMO-PPV films appears to be exciton quenching. All conclusions made in this chapter can be equally applied to both studied materials.

4.1 Thickness dependence of the PL decay

We perform time-resolved measurements of the thin films of pristine material with different thicknesses. It appears that photoluminescence decay is highly dependent on the spin-coat film thickness both for MEH- and MDMO-PPV. A thinner sample demonstrates a faster PL decay. Such dependence is the strongest in the thickness range of 5-100nm. As the thickness increases the effect reaches its "saturation". The photoluminescence decays of samples thicker than 200nm do not differ much with that of drop cast film that is about one micron thick. The thickness effect is comparable with the interface quenching introduced by the poly-(F2D) layer in the heterostructure samples (Fig. 4.1).

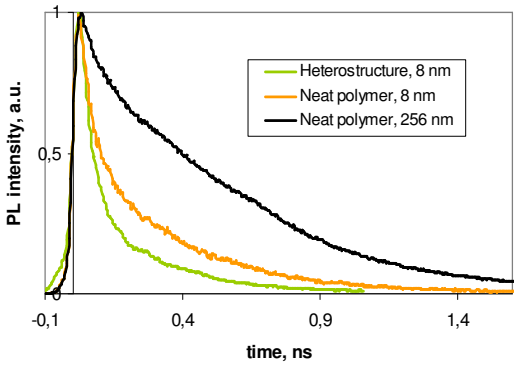

Fig. 4.1 Normalized experimental PL decays measured by TCSPC of samples of different MEH-PPV thicknesses. Measurements were performed at the maximum of the PL spectrum.

In principal the thickness effect can be caused by the process of self-absorption. However the following estimations show that is not true in our particular case. In the process of self-absorption some of the photoluminescence photons are reabsorbed by the material before they leave the film. Obviously the time spacing between the initial excitation and self-absorption is about the exciton life time. Afterwards a new exciton is formed. It lives another lifetime and can emit a photon (with some probability). Thus the resulting light leaves the film after the time of about two exciton lifetimes. The efficiency of self-absorption is determined by the overlap of the absorption and PL spectra (Fig. 4.2a) and by the film thickness. If the contribution of such "delayed" photons is valuable, the resulting PL decay becomes slower in the thicker samples.

Let's estimate the contribution of the self-absorption to the PL decay in our case. Let's suppose that the sample with absorption spectrum $\alpha(\lambda)$ is excited with a pulsed laser. Assuming low absorption coefficient at the excitation wavelength the initial exciton distribution is uniform. The measured PL spectrum $E(\lambda)$ is affected by the self-absorption. Let's denote the unaffected PL spectrum as $E_0(\lambda)$. Upon excitation the volume element $dSdx$ emits light to the observer's direction (Fig. 4.2b) with intensity

$$dE_0(\lambda) = \frac{E_0(\lambda)}{LS} dSdx, \tag{4.1}$$

where S is excited area. Without limitations in general we set $dS = S = 1$.

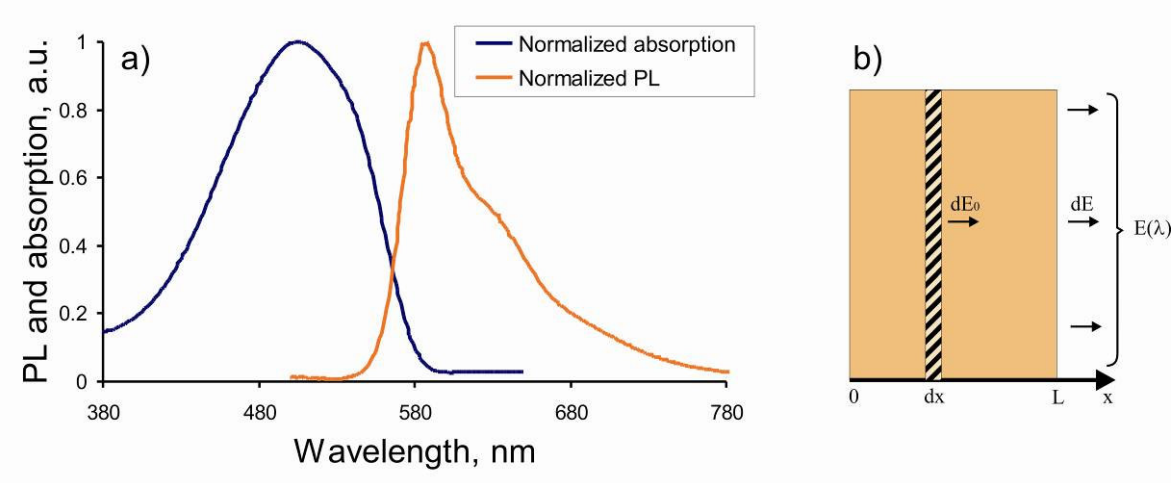

Fig. 4.2 (a) Normalized absorption and PL spectra of 240nm MDMO-PPV. (b) Side view of the polymer film.

Part of luminescence light is reabsorbed by the material. Thus the resulting intensity is

$$dE = dE_0(\lambda)\, e^{-\alpha(\lambda)(L-x)}, \tag{4.2}$$

where L - is the film thickness. The observed spectrum $E(\lambda)$ is then equal to:

$$E(\lambda) = \int_0^L dE = \int_0^L dE_0(\lambda) e^{-\alpha(\lambda)(L-x)} = \frac{E_0(\lambda)}{\alpha L}\left(1 - e^{-\alpha(\lambda)L}\right). \tag{4.3}$$

Thus one can estimate in the first approximation the true spectrum:

$$E_0(\lambda) = \frac{\alpha L E(\lambda)}{1 - e^{-\alpha(\lambda)L}}. \tag{4.4}$$

The number of photons that are reabsorbed is proportional to:

$$n(L) = \int_{\lambda} E_0(\lambda) d\lambda - \int_{\lambda} E(\lambda) d\lambda \tag{4.5}$$

Assuming that all the reabsorbed photons would be reemitted to the observer (upper limit), the contribution to the total intensity of the reabsorbed photons is:

$$\gamma(L) = \frac{n(L)}{\int_{\lambda} E(\lambda) d\lambda}. \tag{4.6}$$

Let's suppose the material have spectrally integrated monoexponential PL decay with a time constant τ in solid state. The PL decay of the thin film with self-absorption can be approximated as biexponential decay:

$$P(t) = A\, e^{-t/\tau} + B\, e^{-t/2\tau}, \tag{4.7}$$

where the second term represents the reemitted photons. Constants A and B can be easily founded by time integration, use of the relationship (4.6) and normalization:

$$P(t) = \frac{2}{2+\gamma} e^{-t/\tau} + \frac{\gamma}{2+\gamma} e^{-t/2\tau}. \tag{4.8}$$

If we consider 240nm thick MDMO-PPV sample we can neglect any surface effects. The value $\gamma(L)$ was calculated numerically based on the experimental data. It is equal to $\gamma = 0{,}03$. Generally speaking the PL decays of MDMO-PPV thin films are not monoexponential. However we can use the expression (4.8) for the visualization of the strength of the effect. Figure 4.3 demonstrates

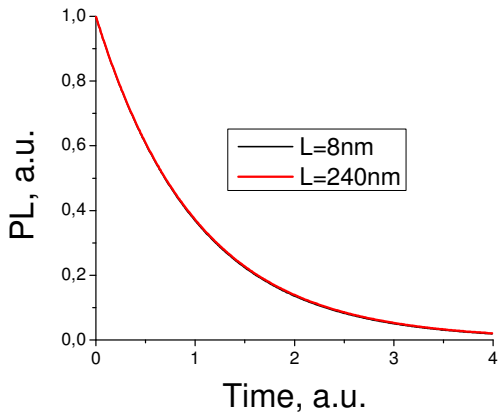

Fig. 4.3. The effect of self-absorption on the thickness dependent PL decay of the MDMO-PPV films is insignificant.

that the effect of self-absorption on the thickness dependent PL decay is insignificant for MDMO-PPV.

4.2 Thickness dependence of absorption and PL spectra

Absorption and photoluminescence spectra were recorded for different polymer spin-cast thin films thicknesses of both types of samples (heterostructures and pristine material) at room temperature (Fig. 4.4). It appears that both spectra depend on the thickness. However the character of the dependences is different. The absorption spectrum first undergoes a red shift on thickness decrease; when the thickness reaches the value of about 15nm the absorption maximum shifts to the blue (Fig. 4.4a).

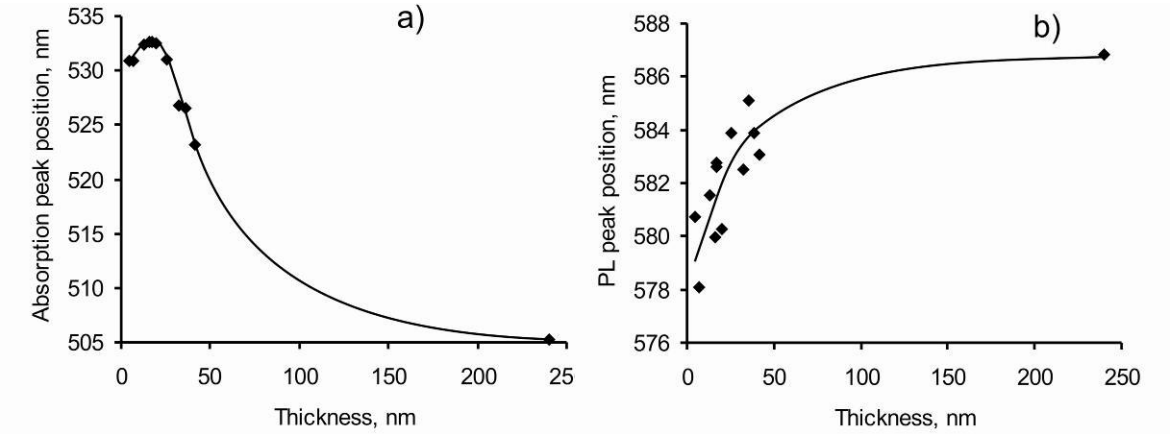

Fig. 4.4. Dependence on thickness of the peak position of absorption (a) and photoluminescence (b) spectra on thickness of MDMO-PPV heterostructures. The positions are determined by the Gaussian fit in the vicinity of the peak. The lines are drawn as guides for the eyes.

The photoluminescence spectrum undergoes blue shift on the thickness decrease (Fig. 4.4b). The dependence is weaker compared to the absorption spectrum, and remarkably has the opposite direction. The photoluminescence peak position was found to be almost the same for both heterostructures and pristine samples of the same thicknesses. Here the data of the heterostructures are presented as measured with the calibrated instrument. The evidences of the blue shift of PL spectrum on decreasing of the thickness can be also founded elsewhere [42].

4.3 Discussion

The red shift of the absorption spectrum indicates the higher average level of conjugation in the thinner samples. Or by other words, the molecular chains are better ordered (on average) in such samples. Further decrease of the thickness leads to the blue shift of the spectrum i.e. the molecular chains of ultra thin (<15nm) films are less ordered on average than somewhat thicker ones. The character of dependence suggests that close to the free interface the film is better ordered than in the bulk (Fig. 4.5). Thus it looks that there are two differently ordered layers in the film. This argument can be intuitively understood from the process of spin-coating. During the spinning the material is escaping the substrate in the lateral direction. One can speculate that escaping solution can somewhat orient the surface of the remaining film.

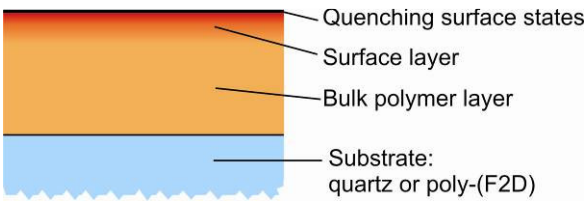

Fig. 4.5. The layered structure of spin-coat PPV film.

The argument of layered structure is also supported by several other experiments. Webster e*t al.* [43] performed **neutron scattering experiments** on MEH-PPV films prepared by the spin-coating technique as well as formed from the precursor. They conclude that spin-coat film had two well-defined layers of different density. While the film prepared by the precursor route was uniform. Even if the neutron scattering experiment did not allow to the authors to make a conclusion concerning the sequence of the layers, the layer thicknesses and approximate densities could be determined. The thin dense layer was about 24nm thick while the thick "spongy" layer had thickness of about 140nm. It is remarkable that the "spongy" layer had density of about one third of that of the thin dense one.

Reflection-absorption Fourier transform infrared spectroscopy with polarized lights was used to demonstrate the bi-layered structure in spin-coated polyacrylaminde (PAL) films [44]. X. Lu *et al.* report that PAL films had two differently ordered layers. For films thinner than about 100 nm no significant spin-coating induced chain orientation was observed. However

for the thicker films a bi-layered structure was formed with the top layer better oriented than the bottom one.

An accurate ellipsometry study has been conducted on thin films of the methyl-substituted ladder-type poly(paraphenylene) (m-LPPP) [45]. J. Sturm *et al*. demonstrated an optical anisotropy on the spin-coat thin films strongly dependent on the film thickness. They summarize that the anisotropy of optical constants is caused by the primary in-plane orientation of the polymer chains. This anisotropy vanishes for the thicker polymer films.

And finally a lot of effort on the study of **thickness dependent thermal transition temperatures** of conjugated polymers has been done in the recent years [46, 57]. These studies also point out to the morphology-related issues in the spin-coat films. For instance, Campy-Quiles *et al.* [46] concludes that the thickness dependent glass transition temperature T_g of some conjugated polymers is characterized by three regimes, namely large thickness bulk samples, for which $T_g = T_g^{bulk}$; intermediate thickness samples for which $T_g > T_g^{bulk}$; and ultra thin samples for which T_g drops again. This tree-regime behavior resembles that of absorption thickness dependence in our experiments. Miyazaki *et al*. [57] reproduced the thickness dependence of the polystyrene T_g by a two-layer model consisting of mobile surface and bulk-like layers with different glass transition temperatures.

If we consider the bi-layered film structure from the point of view of the exciton migration process, the interface between the differently ordered layers constitutes a gradient of the average conjugation length perpendicular to the plane of the film. Such a gradient favors the exciton migration towards the better ordered top layer. This process accompanies the reduction of the excitons' recombination energy. Upon radiative recombination such excitons give rise to photons with lower energy than those in the bulk. According to the absorption spectra measurements the free interface layer becomes important in thin samples. The number of such low energy excitons is expected to be considerable for them. This should lead to a red shift of the photoluminescence spectrum upon thickness decrease. But in reality we

observe the opposite trend. The PL spectrum undergoes blue shift in thinner samples. This means that low energy excitons that end up in the top better ordered layer decay in a non-radiative way. Or, by other words, they are quenched. Defects located at the surface could be responsible for such a quenching.

The argument of the exciton quenching by the free interface is also supported by the time-resolved measurements. As it has been reported in one of the previous paragraphs the PL decay is faster in the thinner films.

To conclude, the free surface of the spin-coat film appears to be exciton quenching interface, as it will be demonstrated below, its quenching efficiency is comparable to that of the poly-(F2D) layer.

CHAPTER 5

Exciton diffusion length – mathematical model

The exciton density was modeled by the one-dimensional continuity equation and solved for 100% interface quenching efficiency. Geometries with one and two quenching interfaces were considered. Analytical expressions for photoluminescence decay and for relative quenching efficiency were derived.

5.1 Statement of the problem

We model the exciton diffusion process by the considering the exciton density evolution in time and space. Let's suppose that a laser pulse is exciting a polymer film with thickness L as it is depicted on the Fig. 5.1. Due to the symmetry the exciton density depends only on the coordinate normal to the film. As discussed in several publications [22, 26, 27] we solve one-dimensional continuity equation:

$$\frac{\partial n(x,t)}{\partial t} = -\frac{n(x,t)}{\tau} + D\frac{\partial^2 n(x,t)}{\partial x^2} - S(x)n(x,t) + G(x,t), \qquad (5.1)$$

where n is the exciton density; τ represents the natural radiative and non-radiative decay processes; D is the exciton diffusion coefficient, $S(x)$

represents the exciton quenching processes; $G(x,t)$ is the exciton generation rate.

Since the ultra fast excitation of the pulsed Ti-Sapphire laser was used, the generation rate $G(x,t)$ can be represented as the initial exciton distribution. In our case the excitation was performed in the high energy tail of the absorption spectra. For example the absorption coefficient of the MDMO-PPV at 400 nm is only $8{,}26\times10^{-4}\,nm^{-1}$. Therefore we assume uniform initial distribution of the exciton concentration:

$$n(x,0) = N_0. \qquad (5.2)$$

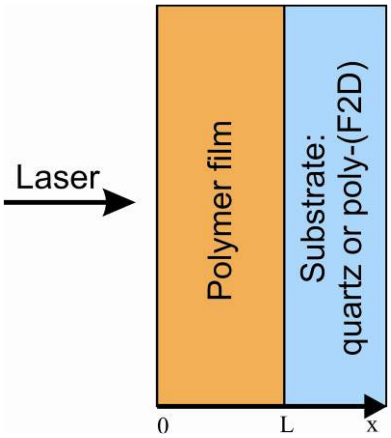

Fig. 5.1. The choice of coordinates.

The exciton quenching term $S(x)$ is geometry dependent. We will solve Eq. (5.1) for different cases. In this paragraph we concentrate on the general approach for the modeling.

Equation 5.1 can be solved analytically for the interface quenching geometries. The resulting exciton concentration is proportional to the number of emitted photons. The proportionality constant is the quantum efficiency ε, which we assume constant for all the samples. Thus the total photoluminescence can be estimated as:

$$PL_{total} = \int_0^L \int_0^\infty \varepsilon\, n(x,t)\,dx\,dt \qquad (5.3)$$

In such a way the relative quenching efficiency (2.2) can be obtained:

$$Q(L) = 1 - \frac{\int_0^L \int_0^\infty \varepsilon\, n_{quenched\ sample}(x,t)\,dx\,dt}{\int_0^L \int_0^\infty \varepsilon\, n_{refference\ sample}(x,t)\,dx\,dt}. \qquad (5.4)$$

As it will be shown below, the one-dimensional exciton diffusion length $L_d = \sqrt{\tau D}$ is the only fit parameter to model this value.

In order to get the exciton diffusion coefficient we model the experimental PL decay with the expression:

$$n(L,t) = \int_0^L n(x,t)dx\,. \tag{5.5}$$

The exciton diffusion coefficient is the only fit parameter here.

5.2 Single quenching interface solution

In heterostructured sample we assume the quenching efficiency of the polymer/poly-(F2D) interface as 100%. This can be expressed by a boundary condition:

$$n(L,t) = 0\,. \tag{5.6}$$

As was demonstrated in the previous chapter, also the free interface of the spin-coat film appears to be exciton quenching surface with unknown efficiency. Therefore we estimate the value of the exciton diffusion length by considering two extreme cases, namely infinite and zero quenching efficiency of the free interface.

The negligible quenching of the free interface introduces the second boundary condition:

$$\frac{\partial n(0,t)}{\partial x} = 0\,. \tag{5.7}$$

The model of one quenching interface can be also applied to the series of the samples of pristine material due to the quenching properties of the free surface.

The boundary conditions (5.6) and (5.7) play a role of the exciton quenching term $S(x)$ in the (5.1). The initial and the boundary conditions simplify the equation (5.1) to a Cauchy problem:

$$\begin{cases} \dfrac{\partial n(x,t)}{\partial t} = -\dfrac{n(x,t)}{\tau} + D\dfrac{\partial^2 n(x,t)}{\partial x^2} \\ n(x,0) = N_0 \\ \dfrac{\partial n(0,t)}{\partial x} = n(L,t) = 0 \end{cases}. \tag{5.8}$$

We seek the solution in the form: $n(x,t) = T(t)X(x)$. Then variables could be separated in (5.8):

$$\frac{1}{T}\frac{\partial T}{\partial t} + \frac{1}{\tau} = D\frac{1}{X}\frac{\partial^2 X}{\partial x^2} = -\lambda^2, \tag{5.9}$$

where λ is a constant. The resulting expression splits into two equations which determines $T(t)$ and $X(x)$:

$$T(t) = e^{-t/\tau}e^{-\lambda^2 t}, \tag{5.10}$$

$$X(x) = ACos(\omega x) + BSin(\omega x), \tag{5.11}$$

where $\omega^2 = \lambda^2/D$. Application of the boundary conditions leads to:

$$\begin{aligned} &B = 0 \\ &\omega_k = \frac{1}{L}\left(\frac{\pi}{2} + \pi k\right), \quad k = 0; \pm 1; \pm 2; \ldots \end{aligned} \tag{5.12}$$

Then the exciton concentration is a linear combination of partial solutions:

$$n(x,.t) = e^{-t/\tau}\sum_{k=0}^{\infty} A_k e^{-\lambda_k^2 t} Cos(\omega_k x). \tag{5.13}$$

Constants A_k are determined by the initial conditions:

$$A_k = \frac{2N_0}{L}\frac{(-1)^k}{\omega_k}. \tag{5.14}$$

The integration on the spatial coordinates finally leads to the photoluminescence decay:

$$n(t) = \frac{2N_0}{L}e^{-t/\tau}\sum_{k=0}^{\infty}\frac{e^{-D\omega_k^2 t}}{\omega_k^2}, \tag{5.15}$$

where $\omega_k = (1/2 + k)\pi/L$.

The relative quenching efficiency is obtained by the time integration of this expression and substitution to (5.4):

$$Q_1(L) = \frac{L_d}{L} Tanh \frac{L}{L_d}. \tag{5.16}$$

The reference sample is considered to be a film with negligible interface quenching. Its total photoluminescence can be easily found to be $PL_{reference} = LN_0\tau$.

5.3 Two quenching interfaces solution

The model of two quenching interfaces can be applied to the heterostructured samples assuming the infinite quenching efficiency of the free interface. The methodological approach for solution of (5.1) is essentially the same as in the previous case. The new boundary conditions are:

$$n(0,t) = n(L,t) = 0. \tag{5.17}$$

The PL decay then looks like:

$$n(t) = \frac{8N_0}{L} e^{-t/\tau} \sum_{k=1}^{\infty} \frac{e^{-D\omega_{2k-1}^2 t}}{\omega_{2k-1}^2}, \tag{5.18}$$

where $\omega_k = \pi k / L$.

The relative quenching efficiency is:

$$Q_2(L) = \frac{2L_d}{L} Tanh \frac{L}{2L_d}. \tag{5.19}$$

An interesting conclusion can be drawn by comparing (5.16) with (5.19). The exciton diffusion length is two times smaller when calculated with the two quenching interface model. This actually determines the maximum error arising from neglecting the effect of the free interface quenching.

5.4 Model assumptions

The quantum efficiency of the exciton – photon conversion ε is assumed to be the same for all the films. The described model does not include the gradient of the conjugation length originating from the two differently ordered layers of the spin-coat film. This gradient is perpendicular to the film and leads rather to a drift of the excitons towards the free interface more than to a diffusion.

CHAPTER 6

Results and discussion

It was demonstrated that the use of heterostructured samples allows getting more accurate results than pristine material samples. The systematic error arising from the morphological issues of the spin-coat film was estimated not to exceed 1 nm. The temperature dependence of the exciton diffusion length (coefficient) was obtained in the range of 4-293K for MDMO-PPV. Upon cooling from room temperature to 100 K the exciton diffusion length (coefficient) drops from 4,7 nm ($3.6 \cdot 10^{-4}$ cm^2/s) to 2,9 nm ($1.5 \cdot 10^{-4}$ cm^2/s) [60]. Further cooling down to 4 K leads to the weak temperature dependence and slight growth up to 3,2 nm ($2 \cdot 10^{-4}$ cm^2/s). The obtained values are an upper limit of the real values mainly due to morphology-related systematic errors. The two temperature regimes showing different trends are qualitatively explained by the quasiequilibrium exciton distribution in an inhomogeneously broadened density of excited states.

6.1 Heterostructures or pristine samples?

The exciton diffusion length measurements in soluble PPV derivatives at room temperature have been previously performed and reported in references [22, 27, 30]. In the present paragraph we concentrate our attention to the morphology-related issues of spin-coat MEH- and MDMO-PPV thin films. The use of time-resolved photoluminescence as in the previous works allows referring to them.

MEH-PPV sample series of the pristine material and the heterostructures with different polymer thicknesses were fabricated as described in Chapter 3. The photoluminescence decays were measured by TCSPC technique on the maximum of the PL spectrum. The deconvoluted data were approximated with three-exponential decays. The dependencies of the relative quenching efficiency (2.2, 5.4) on the thickness have been determined experimentally for the both series. A thick polymer film of about 250 nm has been used as the single reference sample.

The relative quenching efficiency (2.2) of the pristine material series was fit with the single quenching interface model (5.16). In such a way the one-dimensional exciton diffusion length of **7 nm** was extracted. This value could be overestimated due to the assumptions made in the model. First, the real quenching efficiency of the free interface is unknown. The mathematical model assumes 100% quenching. In reality it could be lower. In this case the real value of the exciton diffusion length would be *bigger* than the modeled one. To illustrate this conclusion one can think about the number of excitons that reach the quenching interface, it increases with the exciton diffusion length. A perfect interface quenching means that all those excitons are quenched[1]. If the interface quenching was not perfect, let's suppose 50% efficient, then half of the excitons that reach the interface would be quenched. In order to keep the total number of the quenched excitons constant, the

[1] The number of quenched excitons is measured experimentally. It is proportional to the relative quenching efficiency (2.2).

number of excitons that reach the interface should be doubled. The only way to achieve this is to increase the exciton diffusion length.

On the other hand, the gradient of the mean conjugation length due to differently ordered layers of the spin-coat film could lead to the exciton drift towards the free interface. The drift length is determined by the volume where the gradient is not zero. Such a volume is unknown and probably depends on the sample thickness. The drift leads to the increase of the number of excitons quenched by the free surface. As a result, both the modeled relative quenching efficiency and the exciton diffusion length get higher than physically correct ones. The measured values are surely affected by the gradient effect in our experimental results. However, the assumption about the perfect quenching of the free interface could be true. Data of the heterostructured samples can help to estimate its validity.

The possible systematic errors arising from the assumption of the perfect quenching by the free interface as well as from the exciton drift towards the free interface are reduced by measuring the heterostructured samples. The interface between the polymer and poly-(F2D) could be safely considered as a perfect quencher [20, 21, 28]. The relative quenching efficiency Q (2.2) in fact is the ratio of the quenched excitons q in respect to the number n_0 of emitted photons of the quencher free sample. The number of the quenched excitons is a sum of the excitons quenched by poly-(F2D) q_1 and by the free interface $q_1 - \Delta + \gamma$. The correction Δ is determined by the free interface quenching efficiency: $(q_1 - \Delta)/q_1$; γ is the number of excitons that are brought to the free interface by the drift. Actually Δ and γ introduce systematic errors to the measurements of relative quenching efficiency. The latter is equal to Q' and Q'' for the pristine and the heterostructured samples of the same thickness respectively:

$$Q' = \frac{q_1 - \Delta + \gamma}{n_0} = \frac{q_1}{n_0} + \frac{\gamma - \Delta}{n_0}, \tag{6.1}$$

$$Q'' = \frac{2q_1 - \Delta + \gamma}{n_0} = \frac{2q_1}{n_0} + \frac{\gamma - \Delta}{n_0}. \tag{6.2}$$

The relative systematic errors due to the assumption and the drift are:

$$\eta' = \frac{\gamma - \Delta}{q_1}, \tag{6.3}$$

$$\eta'' = \frac{\gamma - \Delta}{2q_1}. \tag{6.4}$$

Since $|\eta''| < |\eta'|$ the relative quenching efficiency obtained from the **heterostructured samples is more accurate**.

The application of the two interface quenching model to the heterostructured series of samples yields to the exciton diffusion length of **6 nm**. The fact that this value is smaller than the value obtained from the pristine MEH-PPV samples determines the sign of the systematic error $\gamma - \Delta$. The relative quenching efficiency Q_1 (5.16) is monotonically increasing on the exciton diffusion length L_d. Since Q' (6.1) give rise to a value of L_d bigger than the more accurate obtained with the two quenching interfaces then:

$$\gamma - \Delta > 0 \qquad \Leftrightarrow \qquad \gamma > \Delta. \tag{6.5}$$

It means that the systematic error, coming from the assumption of perfect quenching by the free interface, is smaller than the error due to the exciton drift towards the free interface. Since the resulting values are only different for 1 nm the assumption of the perfect interface quenching can be considered as quite lucky.

However, the resulting exciton diffusion coefficient of 6 nm is not free from the systematic errors. The (6.5) indicates that the real exciton diffusion length is smaller than 6 nm. The reduction of the relative error (6.3, 6.4) by a factor of two led to the 1 nm decrease of L_d. The subsequent error reduction would not bring a bigger correction. Thus the real exciton diffusion length is between 5 and 6 nm for MEH-PPV. This result nicely corresponds to works done with similar experimental techniques [22, 27, 30].

6.2 Temperature dependent exciton diffusion parameters of MDMO-PPV

MDMO-PPV is of high interest because it is widely used for the organic solar cells. The described morphology-related effects found for MEH-PPV were also probed with MDMO-PPV at room temperature. The MDMO-PPV appeared to behave very similar to MEH-PPV in this respect. The free interface of the spin-coat MDMO-PPV film also quenches the excitons efficiently. The exciton diffusion length obtained from the pristine samples is bigger than that of the heterostructured samples. This indicates the high efficiency of the free interface quenching as well as the major contribution to the morphology-related systematic error by the gradient of the average conjugation length. Since heterostructured samples lead to more accurate results they were extensively examined at low temperatures.

The time-resolved measurements were performed in the temperature range of 4-293K with a Streak camera working in synchroscan. The spectrally resolved PL decays were wavelength integrated for the data analysis. The resulting decays appeared to be tail cut especially for thicker films because of the instrument limitations (Fig. 6.1). Two-exponential fit was used for their extrapolation. Extrapolated decays where normalized and modeled by the expression (5.18):

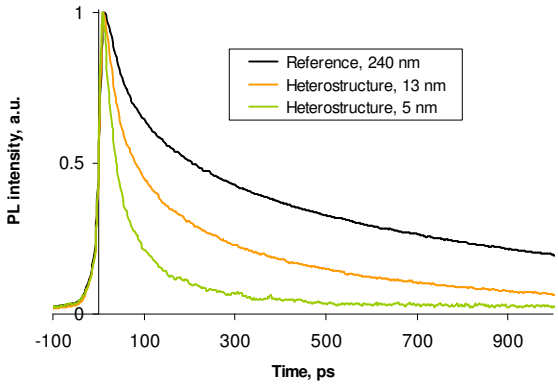

Fig. 6.1. The normalized wavelength integrated PL decays of samples of different MDMO-PPV thickness. Measurements were performed at room temperature in vacuum.

$$n(t,L) = \frac{8}{\pi^2} e^{-t/\tau} \sum_{k=1}^{\infty} \frac{e^{-Dt\pi^2(2k-1)^2/L^2}}{(2k-1)^2}, \qquad (6.6)$$

where L is the polymer film thickness; τ represents the natural PL decay and the exciton diffusion coefficient D is the only fit parameter. The expression (6.6) consists of two time-dependent parts, which have different

physical meanings. The summation represents the exciton diffusion and interface quenching processes. The limit $L \to \infty$ explains the physical meaning of the natural PL decay part:

$$\lim_{L\to\infty} n(t,L) = e^{-t/\tau}. \tag{6.7}$$

It corresponds to the PL decay of a thick film. Since the spin-coat MDMO-PPV film has biexponential PL decay, the expression (6.6) can be approximated as:

$$n(t,L) = \frac{8}{\pi^2}\left(a_1 e^{-t/\tau_1} + a_2 e^{-t/\tau_2}\right)\sum_{k=1}^{\infty}\frac{e^{-Dt\pi^2(2k-1)^2/L^2}}{(2k-1)^2}, \tag{6.8}$$

where a_1, a_2, τ_1 and τ_2 represents normalized PL decay of the thick reference sample at the given temperature. Finally the first 100 terms of (6.8) were used to model PL decays of the samples of different thicknesses (Fig. 6.2a). The mean value as well as the standard deviation was calculated.

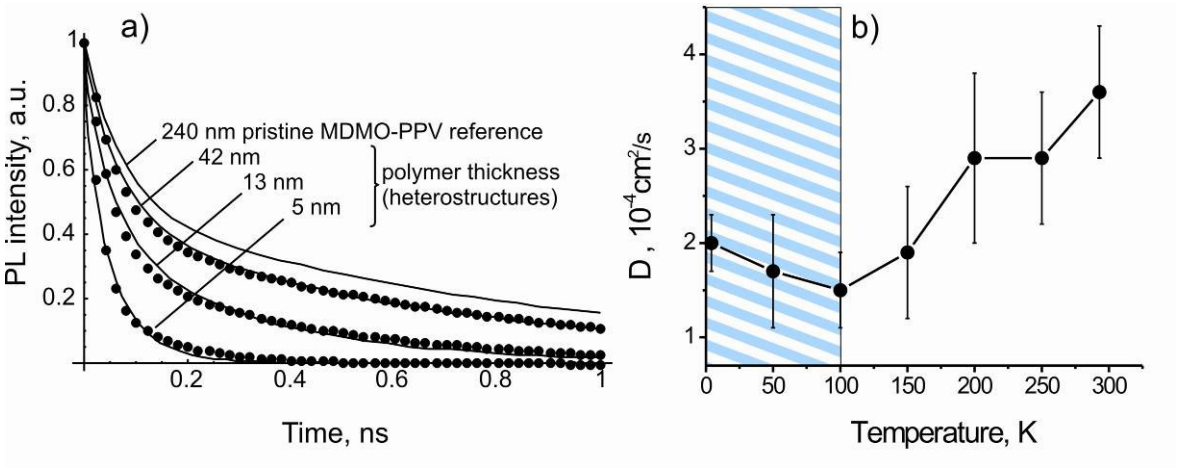

Fig. 6.2 (a) Example of the PL decay fit by Eq. (6.8) for different polymer thickness at room temperature. (b) Temperature dependence of the exciton diffusion coefficient. The error bar is the standard deviation from the mean value of the samples of different thicknesses [60].

The temperature dependence of the exciton diffusion coefficient is depicted on the Fig. 6.2b and summarized in the Table 1.

The exciton diffusion length was obtained by modeling the dependence of the relative quenching efficiency on different polymer thicknesses varying

the exciton diffusion length in the two interfaces quenching model (5.19). The results are presented on the Fig. 6.3 and summarized in Table 1.

Table 1. Summary of temperature dependence of the exciton diffusion coefficient D and exciton diffusion length L_d of the MDMO-PPV. The errors are the standard deviation from the mean value for the samples of different thicknesses [60].

Temperature, K	**D, 10^{-4} cm^2/s**	**L_d, nm**
293	3,6 ± 0,7	4,7
250	2,9 ± 0,7	4,3
200	2,9 ± 0,9	4,3
150	1,9 ± 0,7	3,6
100	1,5 ± 0,4	2,9
50	1,7 ± 0,6	3,1
4	2 ± 0,3	3,2

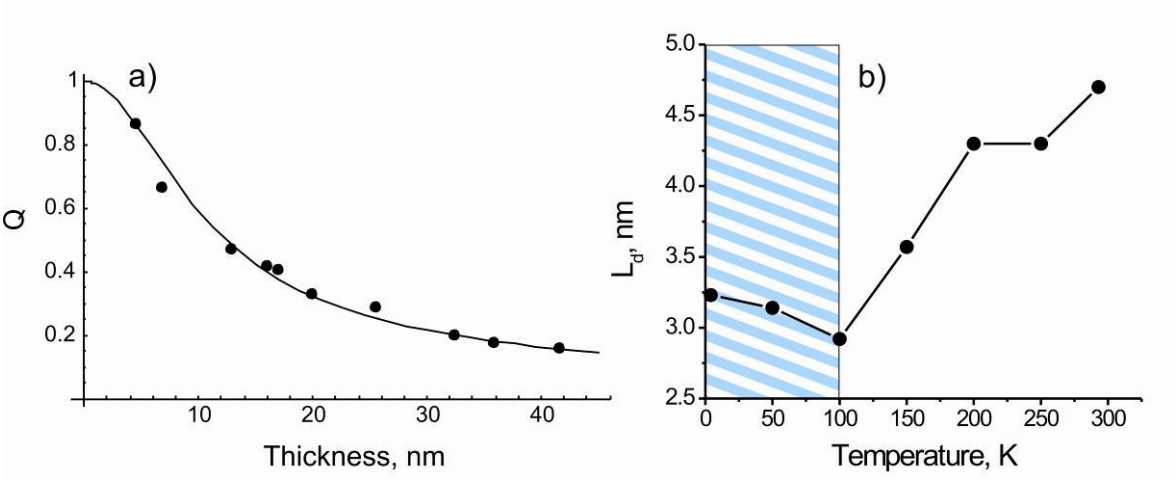

Fig. 6.3 (a) Modeling of the relative quenching efficiency as a function of the polymer thickness at 4K. The black points are experimental data and the curve represent the best model fit with the exciton diffusion length of 3,2 nm. (b) Temperature dependence of the exciton diffusion coefficient [60].

6.3 Discussion

It is remarkable that the temperature dependence of the exciton diffusion length (coefficient) has two different trends. Upon cooling from the room temperature to about 100K it decreases demonstrating thermally activated diffusion. Further cooling leads to a small increase. The measured values – the relative quenching efficiencies (2.2) – depend on both the exciton diffusion length and the free interface quenching efficiency. In principal, the anomalous increase of the estimated exciton diffusion length at low temperatures could be attributed to the possible temperature dependence of the free interface quenching efficiency. We do not expect such dependence to be strong in the studied temperature window because of two experimental facts. First the PL decays' times of thin pristine films always demonstrate the described thickness dependence (see for instance Fig. 4.1). And secondly the values of the exciton diffusion length obtained from the pristine material samples are higher than those obtained from the heterostructured ones for various temperatures. This determines the sign of the systematic error (6.5), which indicates high quenching efficiency of the free interface (about the one of polymer-fullerene interface).

Other arguments could be developed to explain the anomalous trend in the low temperature range (see below). The exciton diffusion length (coefficient) depends on temperature much weaker in such range than in the high temperature range of 100-293K. Such temperature regimes are also presented in the temperature dependence of the PL maximum position as well as in the average PL decay time (Fig. 6.4).

The photoluminescence spectra of MEH- and MDMO-PPV undergo a blue shift on heating (Fig. 6.4a). This phenomenon was previously studied for various PPV derivatives (see [47] and references inside) and several models were developed to describe it. The average conjugation length could decrease upon heating due to the enhancing of torsional movement [49, 50]. This leads to increase of the HOMO-LUMO gap and, as a result, to the blue shift of the maximum of PL spectrum. Such a model fails in several cases. Huang-Rhys

analysis demonstrates that the temperature dependence of the average conjugation length of MEH-PPV can not explain the spectral blue shift [47]. Moreover this model can not be applied to the disordered small molecules with a fixed conjugation length [48].

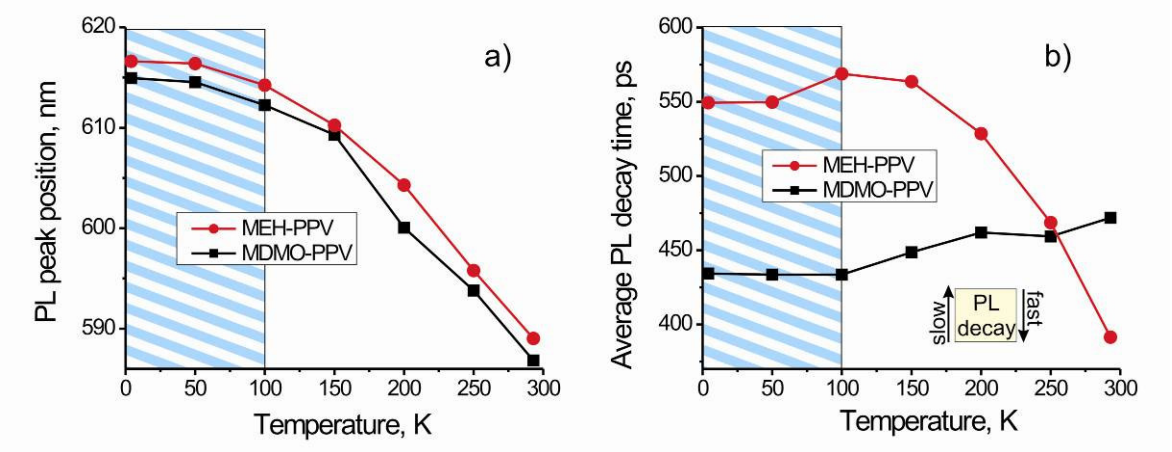

Fig. 6.4 (a) Temperature dependence of the photoluminescence maximum of 240 nm thick pristine samples. It was calculated by the Gaussian fit in the peak vicinity. (b) The average PL decay time demonstrates how fast PL decays under different temperatures.

Wantz *et al.* proposed a model of thermally activated statistic occupation of excited states to describe the temperature dependence of the electroluminescence spectrum in PPV derivatives [47]. The model considers Fermi-Dirac distributions of electrons and holes within the inhomogeneously broadened density of states in the quasiequilibrium approximation. The convolution of those distributions is used to obtain the theoretical temperature dependence of the luminescence spectrum. Such a model sufficiently describes the blue shift of MEH-PPV luminescence spectrum as big as 90 meV in the temperature range of 80-300K; it can be applied for the disordered small molecules; it explains the spectral line broadening upon heating [48]. A similar model was proposed by Anni *et al.* [51]. The thermal quasiequilibrium was described by the Fermi-Dirac distribution of exciton energies within inhomogeneously broadened density of excited states. The exciton migration rate was related to the chemical potential (quasi Fermi level). It was demonstrated that the PL blue shift is mainly due to the increase of the exciton quasiequilibrium temperature. Such a model explains the observed PL temperature dependent shift in poly(9,9-dioctylfluorene) β phase. The

physical picture that is described by such models is summarized as follows. After the excitons creation and their energy relaxation they reach the (thermal) quasiequilibrium that is characterized by an exciton distribution within the density of excited states. The maximum of such distribution depends on temperature, corresponds to the level of the most populated states and is responsible for the maximum of the luminescence spectrum. It moves up in energy on heating leading to the spectral blue shift (Fig. 6.5).

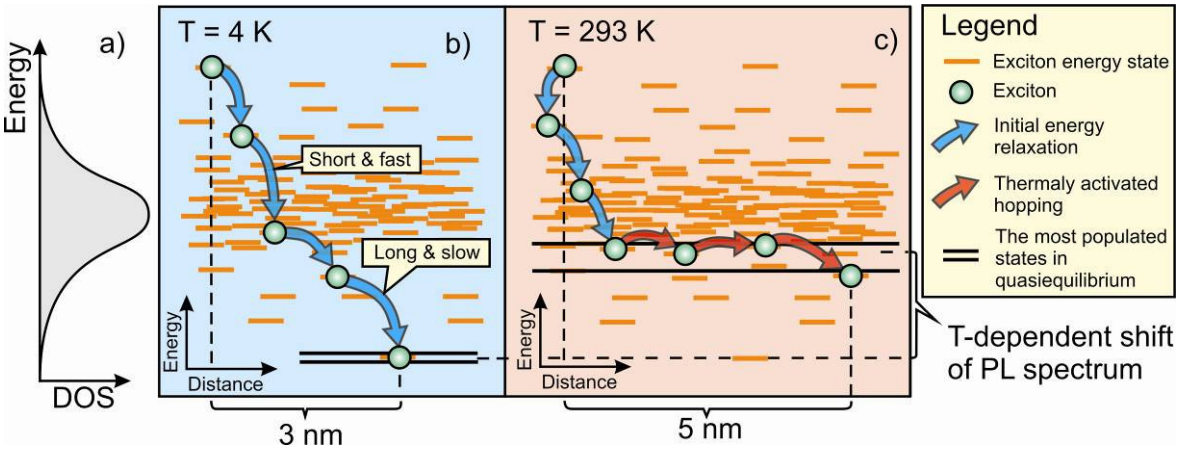

Fig. 6.5. Illustration of the exciton diffusion process under different temperatures. (a) The density of excited states (DOS) corresponds to the statistical energy distribution of the conjugated fragments of various lengths. (b) The initial energy relaxation is responsible for the energy migration process at low temperatures. (c) At high temperatures the thermally activated hopping also contributes to the exciton diffusion length. The T-dependent shift of PL spectrum maximum is shown.

The thermal quasiequilibrium has different properties (meanings) at low and high temperature ranges. Site selective photoluminescence experiment demonstrates those differences. Such experiment studies the dependence of the PL spectrum maximum on the excitation energy [8, 52, 53]. At room temperature the PL spectrum is the same regardless the excitation wavelength. The level of the most populated sites remains in its position even when the excitons are created below it. In this case the excitons gain some energy from the "lattice" in order to reach the thermal quasiequilibrium indicating strong exciton-phonon interaction. Since the level of the most populated states moves up on the DOS tail with temperature increase, the density of such states is relatively high at room temperature. The excitons are fully thermalized and their temperature is equal to that of the

"lattice" in quasiequilibrium [51]. The prefix "quasi" only indicates that such equilibrium is kept during the exciton lifetime.

At low temperature the position of the PL maximum remains constant as long as the excitation energy is bigger than the so-called localization energy. During the energy relaxation excitons hop to lower laying states trying to reach the thermal equilibrium. However at certain exciton energy the concentration of the lower laying states becomes too small i.e. the distance to the nearest target state is too large making the hoping probability insignificant. In this situation the exciton migration process is limited by the localization energy and the excitons are not fully thermalized i.e. they have higher temperature than the "lattice" [51]. Further decrease of the excitation energy leads to exciton creation in the localized sites introducing dependence of the PL spectrum on the excitation wavelength. The exciton-phonon interaction is weak at low temperatures in quasiequilibrium because the exciton can not produce a phonon (for that it should jump to a lower energy state) and it can not absorb a phonon (at low temperature there are not enough phonons). As a result the most populated level is mainly determined by the density of states (if excitation energy > localization energy) and weakly depends on temperature (Fig. 6.4a, 4-100K region). The term "*thermal* quasiequilibrium" does not reflect the physics of the exciton population in this case. The most populated level corresponds to the localization energy, but not to the "lattice" temperature. Therefore a term "*localized* quasiequilibrium" better fits the exciton distribution at low temperatures.

The temperature dependence of the exciton migration also can be explained in terms of quasiequilibrium exciton population. A photon absorption in the high energy tail of the absorption spectrum is followed by the vibronic relaxation and the exciton formation processes. The resulting exciton migrates towards the lower energy sites to reach the localized or thermal quasiequilibrium. At low temperatures the most populated energy sites are located at the bottom of the density of excited states (Fig. 6.5a,b). The energy separation between adjacent sites is high. The excitons can not

migrate any more and eventually they decay radiatively (with some probability) emitting low energy photons. The exciton migration is limited by the *initial energy relaxation* process in this case. The average migration length is determined by the position of the most populated level. As the photoluminescence spectrum measurements (Fig. 6.4a) shows, the latter weakly depends on temperature in the low temperature regime of 4-100K. This leads to the weak temperature dependence of the exciton migration length in such a region (Fig. 6.3b).

Under elevated temperatures the most populated states are located above the bottom of the DOS. If the temperature is high enough such states are quite close in the real space and the energy separation between them is small. In addition, as it was mentioned above, the exciton-phonon coupling is also strong at such temperatures. Therefore a *thermally activated hoping* is possible (Fig. 6.5a,c). Such hopping does not lead to the significant change of the exciton energy. However it contributes the exciton diffusion length. As the temperature increases, the quasiequilibrium level of the most populated sites climbs upwards on the DOS. This leads to the decrease of the average distance between such sites increasing the hopping probability. Thus the exciton diffusion length also increases.

To conclude, the exciton migration process consists of two steps. The initial energy relaxation is the only process at low temperatures. Afterwards, the thermally activated hopping is possible if the temperature is high enough.

Consequently the mechanism of the exciton migration is quite different at low and high temperatures. At low temperatures the exciton migration is not normal diffusion, which is mathematically defined as the variance of a group of random walkers growing linearly in time:

$$\Delta s^2 = Dt, \tag{6.9}$$

where D is diffusion coefficient, and t is time. The variance Δs^2 actually is a square of the diffusion length for the one dimensional diffusion.

The diffusion coefficient for a random walk is expressed by:

$$D = \frac{\langle l^2 \rangle}{\langle \Delta t \rangle}, \tag{6.10}$$

where $\langle l^2 \rangle$ is the average of the square of the hopping length; $\langle \Delta t \rangle$ is the average time between each hop and is determined by the type of the interaction that drives the exciton migration. Possible interactions include Dexter, Förster energy transfers, and more complicated Columbic interactions involving multipoles. However there are evidences that it has mainly Förster-type energy transfer nature [15]. For point-like chromophores:

$$\Delta t \sim \left(\frac{1}{l^6} \right)^{-1} = l^6. \tag{6.11}$$

The important thing is that regardless of the listed energy transfer mechanisms the time between hops Δt depends on the hopping length l differently than the power of two. This makes the exciton diffusion coefficient to be dependent on the average hopping length $\langle l \rangle$. For instance, for the Förster-type energy transfer

$$D = \frac{\langle l^2 \rangle}{\langle l^6 \rangle}. \tag{6.12}$$

For its turn $\langle l \rangle$ depends on the density of target states ρ:

$$\langle l \rangle \sim \sqrt[3]{1/\rho}. \tag{6.13}$$

Thus during the exciton migration down in the density of states the exciton diffusion coefficient is gradually changed from hop to hop i.e. it depends on time. Then the variance (6.9) does not depend on time linearly and such random walk is not a normal diffusion. The described situation corresponds to the initial energy relaxation process. At low temperature such process fully determines the exciton migration, which consequently is not normal diffusion.

The thermally activated hopping happens between sites of similar energy with slightly changing density of states ρ. Thus the average hopping

length (6.13) remains constant during hopping and the variance (6.9) linearly depends on time indicating the normal diffusion.

Consequently the exciton migration process can not be described by the one-dimensional continuity equation (5.1) at low temperatures. A master equation derived for the experimental geometry is more appropriate [54, 55]. In such approach the hopping probability should be estimated, which depends on the energy transfer nature. However, the exact energy migration mechanism is still under debate for polymers. In addition to that master equation requires the exact density of excited states, which is not trivial to derive. The use of such approach will bring extra assumptions and errors. Thus it would not necessary lead to more accurate results.

Due to the strong distance dependence of the energy transfer rate, the energy migration occurs mostly between the nearest neighbors. Therefore the average hop length of an ensemble of excitons is *slightly* changed (first decreased then increased [9, 56]) in time while hopping within the DOS. By applying the normal diffusion approximation we basically average the hoping lengths over the exciton lifetime. Such approximation seems to be reasonable because it sufficiently describes the dependence of the relative quenching efficiency on sample thickness also at low temperatures (Fig. 6.3a). Moreover, Herz *et al.* [56] recently demonstrated that at early times (≤10ps) after the *high energy* excitation diffusion-assisted energy transfer makes significant contribution to the energy migration at low temperatures. This time range is attributed to the energy relaxation trough the DOS maximum. The longer times are characterized by long-range Forster transfer, which is performed in the low energy DOS tail. Thus the validity of the diffusion model is supported by the fact that the described process has essentially diffusion component. The diffusion coefficient of such ultra fast process naturally is expected to be larger than the estimated values (Fig. 6.2), which are averaged over the lifetime.

The described physical picture also explains the temperature dependence of the energy relaxation rate [9, 56]. The average time between

each hop (6.11) gets larger from hop to hop down to the low energy tail of the DOS (6.13). Thus the total relaxation time is longer at low temperatures, when the level of the most populated states is located deeper in the DOS tail. Similar arguments can be used to explain the anomalous growth of the exciton migration length on cooling in the low temperature region. In such a region the thermally activated diffusion is "switched off" and the exciton migration length depends only on the position of the most populated level. The latter is weakly decreasing with temperature shifting to smaller value of density of states. In order to reach it excitons should make a longer hop (6.13) that contributes to the exciton migration length.

Two temperature regimes – above and below 100K – also show up when considering the PL decay times at various temperatures. Figure 6.4b demonstrates how the weighted average PL decay time depends on temperature for both MEH- and MDMO-PPV thick (about 250nm) reference samples. It is influenced by both the nature and concentration of the non-radiative centers – exciton traps and by the exciton diffusion length. The unusual behavior of MDMO-PPV could be explained by the presence of shallow traps within the HOMO-LUMO gap. The trapped excitons could be easily released by the thermal activation. When the sample is cooled down they remain trapped and finally are quenched with the resulting faster PL decay.

An opposite trend is dictated by the probability of reaching a deep trap during the exciton diffusion. Our experimental results show that the exciton diffusion length decreases on cooling, which means that quenching probability by such traps is also decreased. The ratio of shallow and deep traps determines the resulting trend. For instance, the temperature dependence of the PL decay times in MEH-PPV demonstrates mostly deep traps, in contrast to MDMO-PPV, which shows almost equal impact by two different trap types. It is interesting that the signature of the temperature dependence of the exciton diffusion length – two temperature regimes – is presented in the T-dependence of PL decay times of the both materials.

6.4 Thermal expansion

Among the problems of the low temperature experiment there is also the thermal expansion of the films under investigation. There are evidences that the thermal expansion depends on the film thickness [57-59]. Unfortunately it was no possible to measure the film thickness inside the cryostat. In the previously described calculations the thermal expansion was neglected, and the room temperature thicknesses were used for the low temperature modeling.

The relative quenching efficiency Q does not depend on the exciton diffusion length L_d and the polymer thickness L separately (5.19), but on the ratio L_d/L. This value is fixed by the calculation of Q. Due to the fact that we neglect the thermal expansion the modeled value L_d is different from the real $L_d^{(real)}$. The magnitude of this systematic error naturally is determined by the thermal expansion coefficient $\alpha(T)$, relative to the room temperature:

$$L_d^{(real)} = \alpha(T) L_d . \qquad (6.14)$$

Since we expect the thickness to decrease with temperature $\alpha(T) < 1$, then $L_d > L_d^{(real)}$.

The systematic error (6.14) is absent at room temperature and reaches its maximum on minimum of the thermal expansion coefficient $\alpha(T)$ at a low temperature. But since we used quite thin films (5-40 nm) the absolute error due to the thermal expansion is expected to be small.

Finally it is possible to say that there are two systematic errors in our experiment. One is due to the neglecting of the thermal expansion (6.14), another due to neglecting of the gradient of (average) conjugation length (6.4). Both of them make the calculated values of the exciton diffusion length bigger than the real ones. Thus our results correspond to an upper estimation of the exciton diffusion length.

Conclusions

Two differently ordered layers were demonstrated in the spin-coat MEH- and MDMO-PPV films by absorption spectroscopy. The top layer has better ordering and is responsible for the red shift in absorption in very thin films (~15 nm) compared to thick film (100 nm). We found that the free interface of the spin-coat films appears to be exciton quenching for the studied materials with a quenching efficiency comparable to that of fullerene-polymer interface.

The gradient of the average conjugation length is formed at the interface between the differently ordered layers and facilitates the exciton drift towards the free interface. Such a drift introduces a systematic error to the exciton diffusion length calculation, making it bigger than the real value. It was demonstrated that the error is reduced when using heterostructured samples with both quenching interfaces and it does not exceed 1 nm in this case.

The temperature dependence of the exciton diffusion length (coefficient) was measured for MDMO-PPV. It shows two temperature regimes with different trends. Upon cooling from the room temperature to 100 K the exciton diffusion length (coefficient) drops from 4,7 nm ($3.6 \cdot 10^{-4}$ cm^2/s) to 2,9 nm ($1.5 \cdot 10^{-4}$ cm^2/s) [60]. Further cooling down to 4 K leads to a weak temperature dependence and a slight growth up to 3,2 nm ($2 \cdot 10^{-4}$ cm^2/s). Such growth could be attributed to the experimental artifacts, but could also be explained by a qualitative model.

The obtained results are qualitatively explained by the quasiequilibrium exciton distribution in an inhomogeneously broadened density of excited states. The exciton migration process is composed of two steps. Upon the exciton formation the *initial energy relaxation* to the quasiequilibrium level happens. During this process the exciton energy is significantly reduced. At low temperatures (4-100K) such a process fully determines the exciton

migration. If the temperature is high enough (100-293K) the *thermally activated hopping* takes place, which does not lead to large energy relaxation, but contributes the exciton diffusion length.

Acknowledgments

First of all I would like to thank my beautiful supervisor Dr. Maria-Antonietta Loi for the fantastic combination of freedom and nice supervision during my first experience as experimental physicist. You supported all my ideas and at the same time shared your own experience making things work faster. I learned a lot from you during the last year. I thank Prof. Paul Blom for useful discussions during the work meetings and of course for giving me an opportunity to work at the ME-POS group. Also I would like to thank Dr. Bert de Boer for helping me with everything around. A lot of thanks to Frans van der Horst, Jan Harkema and Jurjen Wildeman for giving an excellent technical support. Special thanks to Dorota and Fabrizio, they spent long evenings helping me with low temperature measurements even when Dorota's boyfriend was in Groningen and even if we had to order thick (not Italian for sure) pizza. I thank Afshin, Krisztina, Lacra, Hennie, Victor Malyshev, Ben Hesp and Denis Markov for their time in the lab and useful discussions. Also I thank to the rest of the ME-POS group for friendly environment, which I will have a pleasure to enjoy for the next four years as a PhD student. I would like to thank the Zernike Institute for Advanced Materials for giving me opportunity to participate in the Top Master Program in Nanoscience. Moreover, I would like thank my amazing class-mates Fatemeh, Arramel, Marian, Milo and Asem for a nice time together. And last, but not least, I would like to thank my beloved girlfriend Oksana for the understanding and the great support during my studies in Groningen.

Bibliography

1. L. Zhou, A. Wanga, Sh.-Ch. Wu, J. Sun, *App. Phys. Lett.* **88,** 083502 (2006)
2. H. Sirringhaus, T. Kawase, R.H. Friend, T. Shimoda, M. Inbasekaran, W. Wu, E.P. Woo, *Science* **290,** 2123 (2000)
3. NASA Dryden Helios Photo Collection. http://www.dfrc.nasa.gov
4. C.K. Chiang, C.R. Fincher Jr., Y.W. Park, A.J. Heeger, H. Shirakawa, E.J. Louis, S.C. Gau, and A.G. MacDiarmid, *Phys. Rev. Lett.* **39,** 1098 (1977)
5. U. Rauscher, H. Bässler, D.D.C. Bradley, M. Henneche, *Phys. Rev. B* **42,** 9830 (1990)
6. J.S. Swensen, C. Soci, and A.J. Heeger, *App. Phys. Lett.* **87**, 253511 (2005)
7. J. Zaumseil, R.H. Friend, and H. Sirringhaus, *Nature Mater.* **5**, 69-74 (2006)
8. S. Heun, R.F. Mahrt, A. Griener, U. Lemmer, H. Bässler, D.A. Halliday, D.D.C. Bradley, P.L. Burn, and A.B. Holmes, *J. Phys. Condens. Matt.*. **5**, (1993)
9. B. Mollay, U. Lemmer, R. Kersting, R.F. Mahrt, H. Kurz, H.F. Kauffmann, H. Bässler, *Phys. Rev. B* **50,** 10769 (1994)
10. E.L. Frankevich, A.A. Lymarev, I. Sokolik, F.E. Karasz, S. Blumstengel, R.H. Baughaman, H.H. Horhöld, *Phys. Rev. B* **46,** 9320 (1992)
11. J.W.P. Hsu, M. Yan, T.M. Jedju, L.J. Rothberg, B.R. Hsieh, *Phys. Rev. B* **49,** 712 (1994)
12. I.B. Martini, A.D. Smith, B.J. Schwartz, *Phys. Rev. B* **69,** 035204 (2004)
13. J.J.M. Halls, C.A. Walsh, N.C. Greenham, E.A. Marseglia, R.H. Friend, S.C. Moratti, and A.B. Holmes, *Nature (London)* **376,** 498 (1995)
14. S.E. Shaheen, C.J. Brabec, N.S. Sacriciftci, F. Padinger, T. Fromherz, and J.C. Hummelen, *Appl. Phys. Lett.* **78**, 841 (2001)
15. C.Madigan, V. Bulovic, *Phys. Rev. Lett.* **96,** 046404 (2006)
16. R. Kersting, U. Lemmer, R.F. Mahrt, K. Leo, H. Kurz, H. Bässler and E.O. Göbel *Phys. Rev. Lett.* **70,** 3820 (1993)

17. M.Shielder, U. Lemmer, R. Kersting, S. Rarg, W. Riess, B. Bleve, R.F. Mahrt, H. Kurz, H. Bässler, E.O. Göbel and P. Thomas, *Phys. Rev. B* **54,** 5536 (1996)

18. U. Lemmer, R.F. Mahrt, Y. Wada, A. Greiner, H. Bässler and E.O. Göbel, *Chem. Rev. Lett.* **209,** 243 (1993)

19. G. Cerullo, M. Nisoli, S. Stagira, S. De Silvestri, G. Lanzani, W. Graupner, E. List, G. Leising, *Chem. Phys. Lett.* **288,** 561 (1998)

20. N.S. Sacriciftci and A.J. Heeger, *Int. J. Mod. Phys. B* **8**, 237 (1994)

21. Ch. J. Brabec, G. Zerza, G. Cerullo, S. De Silvestri, S. Luzzati, J.C. Hummelen, S. Sacriciftci, *Chem. Phys. Lett.* **340,** 232 (2001)

22. D.E. Markov, J.C. Hummelen, P.W.M. Blom, and A.B. Sieval, *Phys. Rev. B* **72,** 045216

23. G.S. Kanner, X. Wei, B.C. Hess, L.R. Chen, and Z.V. Vardeny, *Phys. Rev. Lett.* **69,** 538 (1992)

24. B.A. Gregg, J. Sprangue, and M.W. Peterson, *J. Phys. Chem. B* **101,** 5362 (1997)

25. P. Peumans, A. Yakimov, and S.R. Forrest, *J. App. Phys.* **93,** 3693 (2003)

26. Y. Wu, Y.C. Zhou, H.R. Wu, Y.Q. Zhan, J. Zhou, S.T. Zhang, J.M. Zhao, Z.J. Wang, X.M. Ding, and X.Y. Hou, *App. Phys. Lett.* **87,** 044104 (2005)

27. S.R. Scully, and M. D. McGehee, *J. App. Phys*. **100,** 034907 (2006)

28. A. Haugeneder, M. Neges, C. Kallinger, W. Spirkl, U. Lemmer, J. Feldmann, U. Scherf, E. Harth, A. Gugel, and K. Müllen, *Phys. Rev. B* **59,** 15346 (1999)

29. M. Theander, A. Yartsev, D. Zigmantas, V. Sundström, W. Mammo, M.R. Andersson, and O. Inanäs, *Phys. Rev. B* **61,** 12957 (2000)

30. D.E. Markov, E. Amsterdam, P.W.M. Blom, A.B. Sieval, and J.C. Hummelen, *J. Phys. Chem. A* **109,** 5266 (2005)

31. D. McBranch, I. H. Campbell, and D. L. Smith, and J. P. Ferraris, *Appl. Phys. Lett.* **66,** 1175 (1995)

32. C.L. Yang, Z.K. Tang, W.K. Ge, J.N. Wanga, Z.L. Zhang and X.Y. Jian. *App. Phys. Lett.* **83,** 1737 (2003)

33. A.K. Ghosh, D.L. Morel, T. Feng, R.F. Shaw, and Ch.A. Rowe Jr. *J. App. Phys.* **45,** 230 (1974)

34. L.A.A. Pettersson, L.S. Roman, and O. Inganas *J. App. Phys.* **86,** 487 (1999)

35. A.J. Lewis, A. Ruseckas, O.P.M. Gaudin, G.R. Webster, P.L. Burn, I.D.W. Samuel, *Org. Electron.* **7,** 452 (2006)

36. D.E. Markov and P.W.M. Blom, *Phys. Rev. B* **74,** 085206 (2006)

37. G.S. Kanner, X. Wei, B.C. Hess, L.R. Chen, and Z.V. Vardeny, *Phys. Rev. Lett.* **69,** 538 (1992)

38. M. Yan, L.J. Rothberg, F. Papadimitrakopoulos, M.E. Galvin, and T.M. Miller *Phys. Rev. Lett.* **73,** 744 (1994)

39. T. Stübinger and W. Brütting, *J. App. Phys.* **90,** 3632 (2001)

40. L. Lévesque, *Phys. Educ.* **35,** 359-362 (2000)

41. B.M. Ayupov, V.V. Atuchin, T.I. Grigor'eva, L.D. Pokrovskii, and M.S. Lebedev, *Russ. Phys. J.* **49,** 468 (2006)

42. O. Mirzov and I.G. Scheblykin, *Phys. Chem. Chem. Pys.* **8,** 5569

43. G.R. Webster, W.J. Mitchell, P.L. Burn, R.K. Thomas, G. Fragneto, J.P.J. Markham, and I.D.W. Samuel, *J. App. Phys.* **91,** 9066 (2002)

44. X. Lu, I. Cheng, Y. Mi, *Polym.* **48,** 682 (2007)

45. J. Sturm, S. Tasch, A. Niko, G. Leising, E. Toussaere, J. Zyss, T.C. Kowalczyk, K.D. Singer, U. Scherf, J. Huber, *Thin Solid Films* **298,** 138 (1997)

46. M. Campoy-Quiles, M. Sims, P.G. Etchegoin, and D.D.C. Bradley, *Macromol.* **39,** 7673 (2006)

47. G. Wantz, L. Hirsch, N. Huby, L. Vignau, A.S. Barriere, J.P. Parneix, *J. App. Phys.* **97,** 034505 (2005)

48. G. Wantz, L. Hirsch, O.J. Dautel, *App. Phys. Lett.* **90,** 162104 (2007)

49. M. Ariu, M. Sims, M.D. Rahn, J. Hill, A.M. Fox, D.G. Lidzey, M. Oda, J. Cabanillas-Gonzalez, and D.D.C.Bradley, *Phys. Rev. B* **67,** 195333 (2003)

50. F.A.C Oliveira, L.A. Cury, A. Righi, R.L. Moreira, P.S.S. Guimaraes, F.M. Matinaga, M.A. Pimenta, and R.A. Nogueira, *J. Chem. Phys.* **119,** 9777 (2003)

51. M. Anni, M.E. Caruso, S. Lattante, R. Cingolani, *J. Chem. Phys.* **124,** 134707 (2006)

52. H. Bässler, B. Schweitzer, *Acc. Chem. Res.* **32,** 173 (1999)

53. N.T. Harrison, D.R. Baigent, I.D.W. Samuel, R.H. Friend, A.C. Grimsdale, S.C. Moratti, and A.B. Holmes, *Phys. Rev. B* **53,** 15815 (1996)

54. B. Movaghar, B. Ries, M. Grünewald, *Phys. Rev. B* **34,** 5574 (1986)

55. C. Madigan and V. Bulović, *Phys. Rev. Lett.* **96,** 046404 (2006)

56. L.M. Herz, C. Silva, A.C. Grimsdale, K. Mullen, and R.T. Phillips, *Phys. Rev. B* **70,** 165207 (2004)

57. T. Miyazaki, K. Nishida, and T. Kanaya, *Phys. Rev. E* **69,** 061803 (2004)

58. D.J. Pochan, E.K. Lin, S.K. Satija, and W. Wu, *Macromol.* **34,** 3041 (2001)

59. L. Singh, P.J. Ludovice, C.L. Henderson, *Thin Solid Films* **449,** 231 (2004)

60. During the preparation to the publication an imperfection was revealed in the automated process of the analysis of the streak camera data. The improvement led to a sligth change in the resulting values of the exciton diffusion length and coefficient. This change did not influence the main conclusions of this thesis. For the correct values please check
(a) O.V. Mikhnenko, F. Cordella, A.B. Sieval, J.C. Hummelen, P.W.M. Blom, M.A. Loi, *J. Phys. Chem. B.* **112,** 11601 (2008)
(b) O.V. Mikhnenko, F. Cordella, A.B. Sieval, J.C. Hummelen, P.W.M. Blom, M.A. Loi, *J. Phys. Chem. B.* **113,** 9104 (2009)